CENTRO INTERNACIONAL DE ESTUDOS
DE DOUTORAMENTO E AVANZADOS
DA USC (CIEDUS)

TESE DE DOUTORAMENTO

GLOBAL *VS.* LOCAL HEATING IN MAGNETIC NANOPARTICLE HYPERTHERMIA

Cristina Muñoz Menéndez

ESCOLA DE DOUTORAMENTO INTERNACIONAL EN CIENCIAS E TECNOLOXÍAS

PROGRAMA DE DOUTORAMENTO EN CIENCIA DE MATERIAIS

SANTIAGO DE COMPOSTELA

2018

USC
UNIVERSIDADE
DE SANTIAGO
DE COMPOSTELA

DECLARACIÓN DA AUTORA DA TESE

Global *vs.* Local Heating in Magnetic Nanoparticle Hyperthermia

Dna. Cristina Muñoz Menéndez

Presento a miña tese, seguindo o procedemento axeitado ao Regulamento, e declaro que:

1) A tese abarca os resultados da elaboración do meu traballo.
2) De selo caso, na tese faise referencia ás colaboracións que tivo este traballo.
3) A tese é a versión definitiva presentada para a súa defensa e coincide coa versión enviada en formato electrónico.
4) Confirmo que a tese non incorre en ningún tipo de plaxio doutros autores nin de traballos presentados por min para a obtención doutros títulos.

En Santiago de Compostela, a 21 de setembro de 2018

Asdo. Cristina Muñoz Menéndez

USC
UNIVERSIDADE
DE SANTIAGO
DE COMPOSTELA

AUTORIZACIÓN DO DIRECTOR / TITOR DA TESE

Global vs. Local Heating in Magnetic Nanoparticle Hyperthermia

D. Daniel Baldomir Fernández, titor e director
e
D. David Serantes Abalo, director

INFORMAN:

Que a presente tese, correspóndese co traballo realizado por Dna. ***Cristina Muñoz Menéndez****, baixo a miña dirección, e autorizo a súa presentación, considerando que reúne os requisitos esixidos no Regulamento de Estudos de Doutoramento da USC, e que como director desta non incorre nas causas de abstención establecidas na Lei 40/2015.*

De acordo co artigo 41 do Regulamento de Estudos de Doutoramento, declara tamén que a presente tese de doutoramento é idónea para ser defendida en base á modalidade de COMPENDIO DE PUBLICACIÓNS, nos que a participación da doutoranda foi decisiva para a súa elaboración.

A utilización destes artigos nesta memoria, está en coñecemento dos coautores, tanto doutores como non doutores. Ademais, estes últimos teñen coñecemento de que ningún dos traballos aquí reunidos poderá ser presentado en ningunha outra tese de doutoramento.

En Santiago de Compostela, a 21 de setembro de 2018

Asdo. Daniel Baldomir Fernández Asdo. David Serantes Abalo

USC
UNIVERSIDADE
DE SANTIAGO
DE COMPOSTELA

A Lu, mi hermano.

"The only person you are destined to become is the person you decide to be."

- Ralph Waldo Emerson

"Define success on your own terms, achieve it by your own rules, and build a life you're proud to live."

- Anne Sweeney

USC
UNIVERSIDADE
DE SANTIAGO
DE COMPOSTELA

ACKNOWLEDGEMENTS

First of all, I would like to sincerely thank my supervisors Prof. Daniel Baldomir and Dr. David Serantes for allowing me to live the experience of doing a PhD. I would not have increased my scientific knowledge if it were not for them. I would also like to express my deepest gratitude to Prof. Roy Chantrell for welcoming me to his research group and sharing his passion for physics with me.

I would also like to show my gratitude to Dr. Oksana Chubykalo, Dr. Ondrej Hovorka, Dr. Karen Livesey, Dr. Pablo Nieves and all the different people I collaborated with these years for giving me the opportunity to learn from them.

A big thank-you goes to the students in Roy's group who have helped me to improve my skills as a physicist during my research stays in York. I am also grateful to Iván and my IIT colleagues for sharing all these years together.

This work has been funded by Xunta de Galicia and Fondo Social Europeo 2014/2020 (project GRC 2014/013 and the 2016 call of *Programa de Axudas á Etapa Predoutoral*). Additional funding for research stays and trips has been provided by Fundación Barrié (2016 call of *Becas para Estancias Predoctorales en el Extranjero*) and the Royal Society of Chemistry (International Exchanges Scheme - 2016/R2, Standard Programme, IE160535).

This work would not have been possible without the computational facilities and technical support provided by *Centro de Supercomputación de Galicia*.

I also want to show my esteem to all the people on the second floor in the Information Centre whom I met during my stays and trips to York because they turned them worthy and unforgettable.

También quiero expresar mi gratitud a mi familia y amigos, quienes siempre han creído en mí todos estos años. Agradezco a Juan su apoyo en todas las decisiones que he ido tomando en este recorrido. Doy las gracias a María por haber vivido esta experiencia conmigo. Agradezco a Diego que ampliara mi visión sobre esta etapa. Por último, doy las gracias a mis padres. Sin ellos no hubiera llegado hasta aquí.

USC
UNIVERSIDADE
DE SANTIAGO
DE COMPOSTELA

INDEX

USC
UNIVERSIDADE
DE SANTIAGO
DE COMPOSTELA

ABSTRACT

Magnetic nanoparticles (MNPs) dissipate heat when subjected to an external alternating magnetic field. This heat released in the nanoscale has potential uses in a variety of technological fields, ranging from catalysis to nanomedicine. This thesis deals with some not very studied aspects of magnetic nanoparticle hyperthermia (MNH), a new medical technique whose aim is to destroy cancer cells. This is achieved by introducing MNPs into the tumor and heating them by applying an alternating magnetic field. In 2013 MNH received the European regulatory approval for glioblastoma, the most common and aggressive brain tumor in humans and at the moment this technique is available in several German hospitals. However, despite this initial success and its huge potential, MNH has not yet attained a broad clinical application. The goal of this thesis is to investigate some features that are hampering the development of MNH and its translation into the clinics.

It is commonly accepted that for MNH to be effective, the treatment area should achieve a uniform temperature around 43-45°C. Also, to maximize the heating output of the MNPs is considered a key priority in the MNH research field. This way, if MNPs heat more, the dose of magnetic material given to the patient can be decreased. And if tumor temperature reaches appropriate values and is distributed homogeneously, cancer tissue will be harmed without injuring healthy cells. However, two aspects affect these generally agreed upon beliefs about MNH. Firstly, the temperature distribution in the tumor will not be uniform due to the fact that MNPs synthesis techniques cannot totally synthesize monodisperse MNPs both in shape and size. Therefore, each particle with different anisotropy K and volume V will release a different amount of energy E since $E \propto KV$. This causes a distribution of *local* individual particle heating which may be responsible for undesired over- and infra-heating effects in cancer tissue. Besides being an indicator of the maximum attainable heat dissipation, anisotropy K plays a role in determining if the amplitude of the applied field will be able to make the MNPs release energy. In addition, there are some MNH experiments that report cell death without having a global macroscopic temperature variation. A possible explanation may be either mechanical damage or local heat. This second interpretation is supported by several experiments showing huge temperature gradients in the particle surface rapidly vanishing a few nanometers away.

Therefore, this thesis studies variations in local heat caused by polydispersity in size and anisotropy, the link between local (individual particle level) and global (entire system) heat and how they affect the efficacy and safety of MNH. This is done by using a Metropolis Monte Carlo computational technique.

USC
UNIVERSIDADE
DE SANTIAGO
DE COMPOSTELA

1 INTRODUCTION

1.1 Magnetic Nanoparticle Hyperthermia

Magnetic nanoparticle hyperthermia (MNH) is a promising medical treatment that uses the heat generated by magnetic nanoparticles (MNPs) subjected to an external alternating magnetic field H to damage cancer cells by increasing their temperature up to $\approx 45°C$.[1–7] MNH can be used as a stand-alone therapy or as an adjuvant to conventional therapies such as chemotherapy and radiotherapy in order to increase the sensitivity of the tumor cells. This technique is based on the fact that cancer cells are more sensitive to a temperature increase than the healthy ones[1,2,7] and that the magnetic fields necessary to perform MNH do not harm the human body[4,7]. The greatest advantage of MNH is that it is a localized technique: it only affects the tumor area, contrary to radiotherapy or chemotherapy which have undesired secondary effects on the whole body. Therefore, MNH enables to damage cancer cells while having reduced side effects.

1.1.1 Particles and field requirements

To perform an effective and safe MNH treatment, choosing appropriate MNPs and applied magnetic field features is essential.[2–4,7] First of all, MNPs must be biocompatible, non-toxic and stable.[1,4,5,8–10] This is the main reason why iron-oxide based MNPs, especially magnetite (Fe_3O_4) particles, tend to be used.[11] Iron oxides provide the best compromise between good magnetic properties and non-toxicity.[5] Colloidal stability is important to prevent particle aggregation and degradation inside the human body. This is why the iron oxide cores, ranging between a few and tens of nanometers, are coated and functionalized.[5,10]

Several MNPs features are particularly relevant for MNH efficacy and safety:

- Particle size and shape can greatly affect MNPs magnetic behavior.[1,2,4,5,8] Particles must have appropriate size for effective cell internalization. If MNPs are too big, they will tend to aggregate[7] and they will not be able to go through the capillary system of organs and tissues.[10] If they are too small, their heating ability will decrease and they will enter in cells in a non-selective manner.[5] Particle shape together with aspect ratio are relevant features for MNPs cell internalization and heating properties as well.[1,8,12] Elongated structures enhance blood circulation time and increase particle retention in the tumor in comparison with spherical MNPs.[13] Cube-shaped MNPs have a higher heating ability than spherical MNPs[14] whereas nanorods provide greater heating values than cubed MNPs.[15] In addition, particle shape also determines the effective anisotropy of the particles K_{eff}. This is a crucial aspect for MNH because the energy released by the particles is proportional to their volume V and anisotropy constant K: $E \propto KV$.[2,5,7,16]

- Magnetic anisotropy K is therefore another key parameter[17] since it is not only related to the maximum achievable heat dissipation,[17] but also to the necessary amplitude of the applied field to start causing heat dissipation[4,5] and to the sensitivity to dipolar interaction[4]. There are several types of anisotropies in MNPs, being magnetocrystalline and shape anisotropy the most relevant ones.[18] Magnetocrystalline anisotropy arises from the electronic structure of the material, it is the material intrinsic anisotropy. The magnetostatic energy gives rise to the shape anisotropy. Usually an effective anisotropy constant K_{eff} is used, which includes both magnetocrystalline and shape anisotropy.[19] It is important to recall that without magnetic anisotropy and assuming negligible precession effects, MNPs are anistheretic. A relevant parameter is the anisotropy field, which is defined as $H_A = 2K/M_S$ being M_S the saturation magnetization. It represents the maximum achievable coercive field in the Stoner-Wohlfarth model[20] and it is used as an indicator of the capability of the applied field to make MNPs release energy.

- The homogeneity of the system is also an important aspect to consider. If MNPs have different characteristics, their reaction to the same external stimulus may vary significantly. This could lead to a variety of heating performances within the same sample. Given that size polydispersity is unavoidable by current synthesis techniques and that heating is proportional to particle volume, size dispersion is crucial[1,2,4,7,8] and will be one of the key points of this work. The same happens for anisotropy polydispersity given the double role of anisotropy explained in the previous paragraph. In general, low size dispersion is preferred in order to have a better control of the magnetic behavior of the material.[4]

- Particle concentration $c = V_{MNPs}/V_{system}$, where V_{MNPs} is the total volume occupied by the MNPs and V_{system} is the total volume of the system, is important too. Concentration regulates the strength of the magnetic interactions among MNPs, which can cause a broad variety of heating responses.[2,21] Behaviors of interaction diminishing,[14,22–24] enhancing[25–28] and both increasing and decreasing[16,21,29,30] MNPs heating performance have been observed. Discrepancies are attributed to field amplitude,[16,21] temperature,[29] ability for chain formation[27,28] and possible interplay of particle size, anisotropy and temperature[30].

In general, the heating ability of MNPs is determined for particles in solution.[31] Therefore, two mechanisms can be the cause of heat dissipation: magnetization reversal over the energy barrier and physical rotation of the MNPs within the viscous liquid environment, the so-called Néel and Brownian relaxation respectively. The Néel contribution refers to the inner magnetization reversal over the anisotropy energy barrier E_B whereas Brown reversal stands for the physical rotation of the entire particle within the embedding viscous environment.The average time τ that the magnetization takes to overcome the energy barrier due to thermal fluctuations follows an Arrhenius law:[32,33]

$$\tau = \tau_0 e^{\frac{E_B}{E_{th}}}. \tag{1.1}$$

τ_0 is the attempt time and usually ranges between 10^{-9} and 10^{-11} seconds. The measurement time τ_m differentiates the ferromagnetic regime, where $\tau_m << \tau$ and MNPs are blocked, and the superparamagnetic regime, where $\tau_m >> \tau$ and the average magnetization is zero. Blocking temperature T_B defines the transition between both regimes, at $\tau_m = \tau$:

$$T_B = \frac{E_B}{k_B ln(\tau_m/\tau_0)}. \tag{1.2}$$

The Brownian relaxation time is defined as $\tau_B = 3\eta V_h/E_{th}$, where η is the viscosity of the environment and V_h is the hydrodynamic volume of the particle.[34,35] Regarding clinical application of MNH, the key is to evaluate the heating performance of MNPs in cellular media.[31] In this case and as it will be explained in the physical model 1.3.2 later, Brownian contribution can be neglected. However, the fact that Brownian relaxation can be disregarded as a heating mechanism for MNPs in the cellular environment does not imply that it may contribute by enabling the reorientation of the easy axes of the MNPs.[36,37]

Field frequencies for MNH usually range between 100 and 500 kHz.[4] Field amplitudes for MNH usually go from 200 to 600 Oe.[4] Regarding the safety of applying an external applied magnetic field, Brezovich and coauthors[38] suggested that the upper limit for the product of magnetic field amplitude H_{max} and frequency f should not exceed $4.85 \cdot 10^8$ A/m·s. This criterion was established by subjective pain perception of volunteers exposed to magnetic fields. More recent works suggest that the product $H_{max} \cdot f$ can surpass the previous established limit without harmful side effects.[39,40] Also, Ref. 2 suggests to consider the $H_{max} \cdot f$ limit as $5 \cdot 10^9$ A/m·s. Another requirement is that the alternating magnetic field generators for MNH have to be able to create a homogeneous field intensity in the treatment area.[4] Achieving this considering that the current used coils surround the human body[41] is particularly challenging from the engineering point of view. As it can be seen, optimizing MNH is a complex task and requires effort from different fields such as biology (MNPs interact with the human body), medicine (it is necessary to develop clinical protocols to implement MNH), chemistry (particle synthesis and functionalization), physics (MNPs heating capabilities) and engineering (appropriate devices for clinical implementation of MNH).

1.1.2 State of the art

MNH has received the European regulatory approval in 2013 for glioblastoma and is currently available in various German hospitals. Several clinical trials have been done in Germany for glioblastoma multiforme,[42–44] the most aggressive and common brain tumor in humans, prostate cancer[45–47] and other solid tumors such as cervical or ovarian ones.[48] There is one clinical trial going on in London for prostate cancer[49] and another one planned in the US.[41] Another clinical trial for subcutaneous tumors such as breast cancer, head and neck tumors or oral cavity tumors is taking place in Japan.[50]

The most remarkable example of success in using MNH is MagForce AG,[41] a German company founded in 1997 which also developed the first alternating field applicator for humans.[1] They have clinically tested MNH on about 80 patients with brain tumors, 30 with prostate cancer and approximately 40 patients with other type of tumors (esophageal or pancreatic, for

instance). Regarding glioblastoma, MNH has increased survival after first tumor recurrence from 6 to 13 months and after primary tumor diagnosis from 14 to 23 months.[43]

Physicians use a ferrofluid consisting of aminosilane coated magnetite particles (roughly 12 nm of core and 3 nm of coating) dispersed in water. Iron concentration is approximately 112 mg/ml. They first perform a multiple injection of this ferrofluid into the tumor (0.3 ± 0.1 ml of ferrofluid per cm^3 target volume), where the separation among the injection canals does not exceed 10 mm. The objective is to obtain a highly homogeneous particle distribution. Then, once they know particle location in the tumor, they estimate the necessary amplitude of the applied magnetic field to reach treatment temperatures by doing simulations using the bioheat transfer equation. The field strength provided by their coils can reach approximately 200 Oe. The frequency of the field is fixed to 100 kHz. MagForce usually performs one hour sessions twice per week during three weeks. MNPs delivered to the tumor stay in the treatment area so it is only necessary to inject them once.

1.2 DIFFICULTIES AND MOTIVATION

Despite its great potential and advantages in relation to conventional cancer treatments, MNH has not reached a broad clinical application. Several plausible reasons are envisaged. For instance, particle behavior changes depending on the media they are dispersed in. Thus it is not the same to study and try to optimize particle features *in vitro* than their later actual behavior *in vivo*.[2,4] Also, MNPs tend to degrade in a biological environment[1,4,5,8] and their heating properties change[4]. In addition, cell death mechanisms related to a localized increase of temperatures are not yet well understood.[5]

The main problem regarding the underlying physics is that there is a lack of an accurate control of the MNPs heating performance. As mentioned before, a lot of parameters (MNPs characteristics and experimental conditions) affect the heat released by the particles and there are intertwined effects. Therefore, it is not easy to optimize MNPs features for MNH. The fact of not controlling precisely the MNPs heating behavior has crucial efficacy and safety implications: on the one hand, if heat is not enough, the tumor cells will not be sufficiently damaged and the treatment may not be as effective as desired. On the other hand, if there is a heat oversupply, surrounding healthy tissue may be wounded.[4–7] Particle dose and particle spatial distribution in the tumor will have a significant effect in this regard.

The motivation for this work arises from the need to improve the control of MNPs heating performance combined with the fact that several studies may challenge two commonly accepted ideas regarding the way to improve MNH. These generally agreed upon beliefs are:

- A homogeneous temperature distribution should be attained and kept inside the tumor during the MNH treatment.[1,2,7] This way all the tumor area would be handled equally and, if the heat dose is adequate, cancer cells would be damaged while preserving healthy tissue.

- The higher the heat released by MNPs, the better. Since physicians recommend to introduce the smaller amount of MNPs inside the body as possible, MNH research tends to

focus on enhancing the heating capability of the MNPs so the heating is maximized and the necessary doses can be lowered.[1,4,5,7]

There are two problems with the first point. One is the feasibility of the notion: despite a proper magnetic material dose is injected, a nearly homogeneous particle distribution is attained in the tumor and appropriate applied field parameters are selected, the temperature distribution will not be uniform. This is because MNPs synthesis techniques are not able to synthesize completely monodisperse samples, both in size and shape. Recalling that the energy released by a particle is proportional to its anisotropy constant and volume ($E \propto KV$, where aspect ratio is directly linked to K[12]), each particle will supply a different heating output. Accordingly, there will be an unavoidable variety of *local* heating spots. Here *local* refers to the nanoparticle environment. *Local heat* contrasts with *global heat*, which is the macroscopic heat usually measured. The diversity in local heating may be very relevant for MNH efficacy and safety, as illustrated in Fig. 1.1: two samples of MNPs release the same amount of global energy but with an entirely different local heating output because of having different size dispersion degrees.

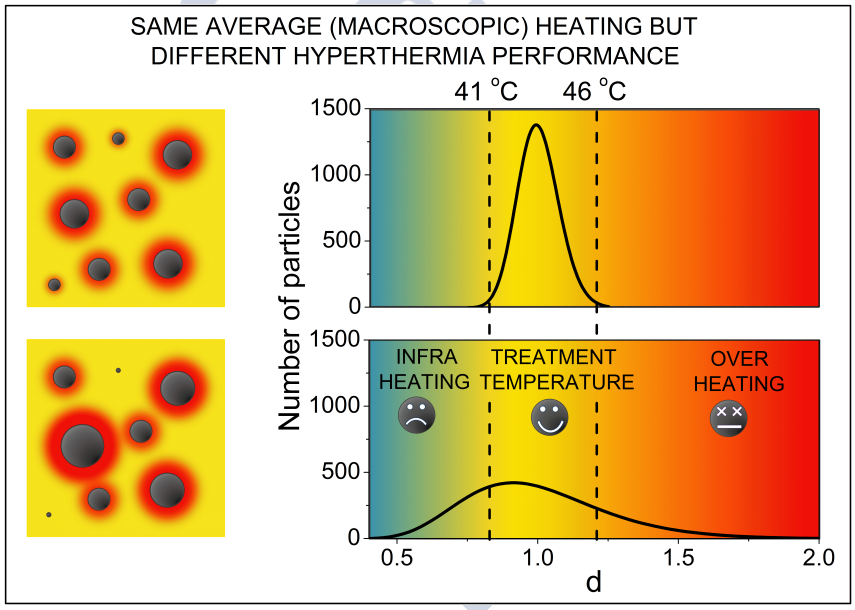

Figure 1.1: Scheme of two size polydisperse samples with possible corresponding size distributions. The color scale is used to show that size polydispersity may cause local over- and infra-heating effects because part of the MNPs are releasing energy outside the desired heating range. [This figure can be found in the link of Ref. 51 as the graphical abstract of paper 1 (see chapter 5).]

The second issue affects the two aforementioned common beliefs for MNH and demonstrates the need to study local heating: *there are several MNH experiments reporting cell death without measuring a macroscopic temperature increase*.[52–55] These works clearly challenge the presumed need of achieving a significant global temperature increase to have MNH efficacy. In addition, the quest for enhancing global SAR values as much as possible might need

to be reconsidered. Also, the mechanism leading to cell death in these MNH experiments deserves further attention. One possible explanation could be that mechanical damage may kill the cells. Another option is that local heat precipitates cell apoptose. This last option is supported by the huge local temperature gradients observed in Refs. 56–58. These experiments report an increase of tens of K in the particle surface in relation to the global measured temperature. Interestingly, global temperature is recovered just 5 nm away from the particle surface.[57] Thus, having cell death triggered by local heating and without a global increase of temperature emerges as a plausible option.

The preceding arguments show that studying local heating in the framework of MNH is significant, suitable and necessary. Therefore, this thesis focuses on investigating local heat effects due to K and V polydispersity, how they relate to global heating and how they affect the efficacy and safety of MNH. This is the line of reasoning of this thesis, which provides coherence and unity to it and its parts. This work contains the following steps: Firstly, the influence of size polydispersity is examined. Then, a theoretical method on how to choose average particle size to improve MNH effectiveness taking into account local heat and size dispersion is developed. Finally, the effect of having an anisotropy dispersion and its connection with the amplitude of the applied field H_{max} and a better MNH treatment is evaluated. These objectives are further explained in chapter 2.

1.3 METHODOLOGY

To investigate local heating effects in an ensemble of MNP for MNH, computational simulations will be performed. Modeling does not only help to understand experimental observations and optimizing MNPs parameters,[4] but is also considered to be a key priority to facilitate the transfer of nanomedicine from the laboratory to the clinic[3]. A Monte Carlo technique with a Metropolis algorithm[16,59,60] is used to simulate magnetization M *vs.* applied field H hysteresis loops and calculate the Specific Absorption Rate (SAR). A Monte Carlo simulation denotes a calculation that integrates over a random sampling of points instead of a regular array of points.[59] This kind of technique is useful for complex and/or high-dimensional problems. Calculations for this work need to be done in a 3D space (each MNP has its own x, y and z coordinates) and for a large number of particles. Therefore, the suitability of the aforementioned simulation technique for achieving the objectives of this thesis is justified.

1.3.1 Specific Absorption Rate (SAR)

The magnitude commonly used to report MNH heating capabilities is the Specific Absorption Rate (SAR),[1,61] also known as Specific Loss Power (SLP) or Specific Heating Power (SHP)[4]. SAR is defined as the rate at which electromagnetic energy is absorbed by a unit mass of a magnetic material and is usually reported in W/kg units.[61] SAR can be obtained by multiplying the area HL of the hysteresis loop, which stands for the hysteresis losses, by the frequency of the applied field f as[6,17,18]

$$SAR = HL \cdot f. \tag{1.3}$$

This value is usually assumed to be equivalent to the SAR estimated from the initial slope of the heating curve measured in adiabatic conditions[1,61] as[62,63]

$$SAR = C_{sample}\frac{m_{sample}}{m_{MNPs}}\frac{\Delta T}{m \cdot t}. \tag{1.4}$$

C_{sample} is the heat capacity of the sample, ΔT is temperature variation, m is mass and t is time. Given Eq. 1.3 and unless otherwise specified, the hysteresis losses HL are treated as an equivalent to SAR.

1.3.2 Physical model

The physical model considered consists of N single domain MNPs with the atomic moments of each particle rotating coherently. Therefore, each particle i can be described by a magnetic moment $\mu_i = M_{S_i}V_i$ (this is the macrospin approximation), effective uniaxial magnetic anisotropy K_i and easy axis direction $\hat{n}_i$, which is distributed randomly. M_{S_i} is saturation magnetization and V_i is particle volume. Brownian relaxation is not taken into account because there are MNH experiments reporting an insignificant[64] or even a non-existing[31,65] effect of it on MNH performance in cellular environment. Thus, particles are immobilized and are not allowed to rotate.

The total energy E_{tot} of the system has three contributions: Zeeman $E_Z(i) = -\vec{\mu}_i \cdot \vec{H}$, anisotropy $E_K(i) = -K_iV_i(\hat{\mu}_i \cdot \hat{n}_i)^2$ and dipolar $E_D(i,j) = \frac{\vec{\mu}_i \cdot \vec{\mu}_j}{r_{ij}^3} - 3\frac{(\vec{\mu}_i \cdot \vec{r}_{ij})(\vec{\mu}_j \cdot \vec{r}_{ij})}{r_{ij}^5}$, where $\vec{r}_{ij}$ is the vector connecting the particles in positions $\vec{r}_i$ and $\vec{r}_j$. Accordingly, the total energy of the system is:

$$E_{tot} = \sum_i \left[E_K(i) + E_Z(i) + \frac{1}{2}\sum_{j \neq i} E_D(i,j) \right]. \tag{1.5}$$

Total magnetization is calculated differently depending on the type of polydispersity considered. If there is anisotropy dispersion, the total magnetization of the sample in the direction of the applied field is

$$M = M_S V \sum_{i=1}^{N} cos\theta_i, \tag{1.6}$$

where θ_i is the angle between the magnetic moment of particle i and the applied field $\vec{H}$. N is the number of particles of the sample, which is 2000 for all the calculations. If size is dispersed, the total magnetization is

$$M = M_S \sum_{i=1}^{N} V_i cos\theta_i. \tag{1.7}$$

Polydispersity is simulated by creating size and anisotropy categories and then assigning particles to them so they follow a desired distribution. Particle diameters D follow a lognormal size distribution because this is what experiments[16,63,66–70] usually report:

$$f(D;U,\sigma) = \frac{1}{\sqrt{2\pi}D\sigma} e^{-\frac{(\ln(D)-U)^2}{2\sigma^2}}. \tag{1.8}$$

σ is the standard deviation of $\ln(D)$ and U is the average of the logarithms of the diameter.

Similarly, a normal anisotropy distribution[12] of average $\langle K \rangle$ and standard deviation σ_K was considered:

$$f(K;\langle K \rangle,\sigma_K) = \frac{1}{\sqrt{2\pi}\sigma_K} e^{-\frac{(K-\langle K \rangle)^2}{2\sigma_K^2}}. \tag{1.9}$$

For the simulations, discrete distributions are implemented. This way, size and anisotropy categories are created. Each category j has a number of N_j particles having the same diameter D_j or anisotropy K_j. In order to discern effects arising from size and anisotropy polydispersity, either a size or an anisotropy dispersed sample is considered. Therefore, simulations with both parameters distributed simultaneously are not considered.

Working in dimensionless units allows for generality: the simulations are useful for predicting and interpreting results of different materials (variation in M_S and K), sizes and applied field conditions.[1] Accordingly, normalized units will be used from now on unless otherwise specified.

The diameter D is normalized to the diameter of the ideal monodisperse system D_0 as $d = D/D_0$.[2] The average diameter of the polydisperse system $\langle D \rangle$ is taken as D_0. Therefore, $\langle d \rangle = \langle D \rangle / D_0 = 1$. Similarly, anisotropy K is normalized to the anisotropy of the ideal monodisperse system as K/K_0.

Magnetization is normalized by $M_S V_{tot}$. Therefore, magnetization is simply written as $M/M_S V$ for both global and local cycles if anisotropy dispersion is considered. However, the notation changes when considering size dispersion: if the loop is global, the magnetization $M/M_S V_t^0$ is used, where$V_t^0 = NV_0$ is the total volume of the monodisperse sample. If the cycle is local, then the magnetization of a size category $d_j = D_j/D_0$ is represented with notation

$$\mathscr{M}_j = \frac{v_j}{N_j} \sum_{k=1}^{N_j} cos\theta_{kj}. \tag{1.10}$$

$v_j = V_j/V_0$ is category volume and θ_{kj} is the angle between the magnetic moment of particle k in category j and the applied field. Normalized total magnetization for a size polydisperse sample can be therefore naturally written as

$$\frac{M}{M_S V_t^0} = \frac{1}{N} \sum_{i=1}^{N} v_i cos\theta_i = \frac{1}{N} \sum_{j=1}^{P} \left(v_j \sum_{i=1}^{N_j} cos\theta_i \right) = \frac{1}{N} \sum_{j=1}^{P} N_j \mathscr{M}_j, \tag{1.11}$$

[1] It is important to remark that the parameters (size, for instance) must respect the physical model with its approximations and validity conditions when translating dimensionless results into real units. For example, since the macrospin approximation is assumed, equivalent sizes in real units cannot be so large that non-coherent reversal processes are allowed.

[2] D_0 is both the particle diameter and the average diameter of the monodisperse system.

with $v_i = V_i/V_0$ being the volume of particle i and P the number of categories considered. The maximum value of P is 25.

Hysteresis cycles are presented in normalized fiels units: $h = H/H_A$ if there is size polysipersity and $h = H/\langle H_A \rangle$ if there is anisotropy polydispersity. Some hysteresis loops for a size polydiserse system are shown in Fig. 1.2. The scheme illustrates a sample with size dispersion and the influence of particle volume on individual particle heating ability. The global cycle is shown with its corresponding magnetization and field notation. Three local hysteresis loops for three different particle volumes are depicted. They illustrate the fact that, at local level, magnetization $\mathscr{M}_j$ can vary between $-v_j$ and v_j (see Eq. 1.10). Also, they show how local hysteresis losses hl_j scale with volume v_j. In Fig. 1.2, each category has the same coercive field. This is because very low temperature was considered. If temperature is increased, the local coercive fields will be different depending on how big is the thermal energy $E_{th} = k_B T$ (being k_B the Boltzmann constant and T the temperature) in comparison with the energy barriers.

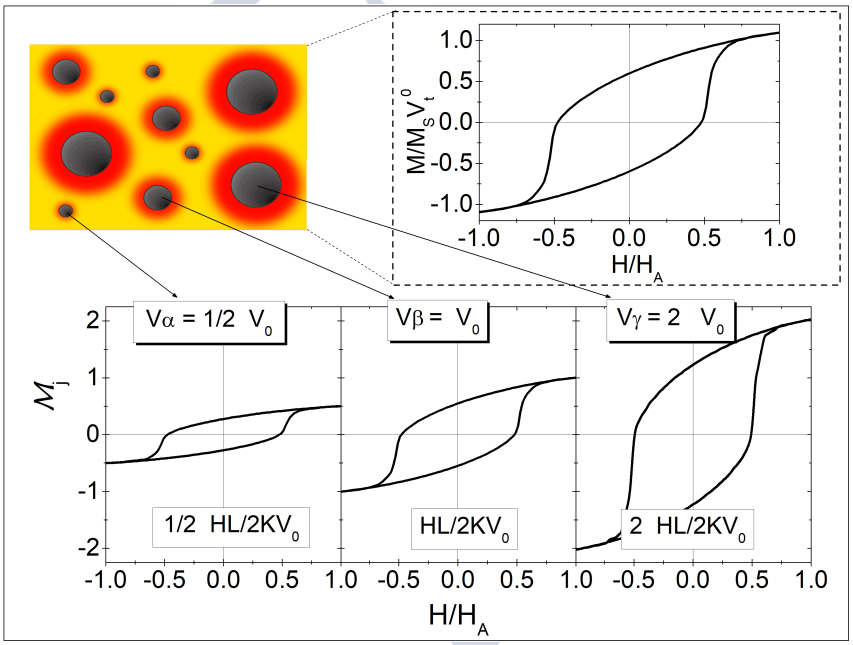

Figure 1.2: The hysteresis cycle of an entire size polydisperse system is shown together with three hysteresis loops corresponding to three different particle sizes. [This figure belongs to paper 1 in chapter 5.]

The area of the loops is normalized to the maximum achievable power for an ensemble of randomly distributed MNPs following the Stoner-Wohlfarth model, which is $HL^0_{max} = 2KV^0_t = 2KNV_0$. Thus, global hysteresis losses are reported as $hl = HL/HL^0_{max}$ (so $hl^0_{max} = 1$) and the local ones as $(hl)_j = (HL)_j/HL^0_{max}$. Temperature is also given in normalized units as $t = k_B T/2KV_0$.

Likewise volume, hysteresis losses scale with anisotropy. Fig. 1.3 A indicates that the hysteresis loops scale with the normalized field h for different anisotropy values. The x-axes

for each case show that each cycle is the same if it is plotted against its own H_{max}/H_A field. Fig. 1.3 B reflects the double role of the anisotropy as explained in subsection 1.1.1, both delimiting the maximum achievable heat and establishing the necessary field amplitude so that dissipation starts to be relevant. It also illustrates that the data would collapse into the same curve if the normalization for HL and H_{max} was done in relation to the anisotropy value of each sample.

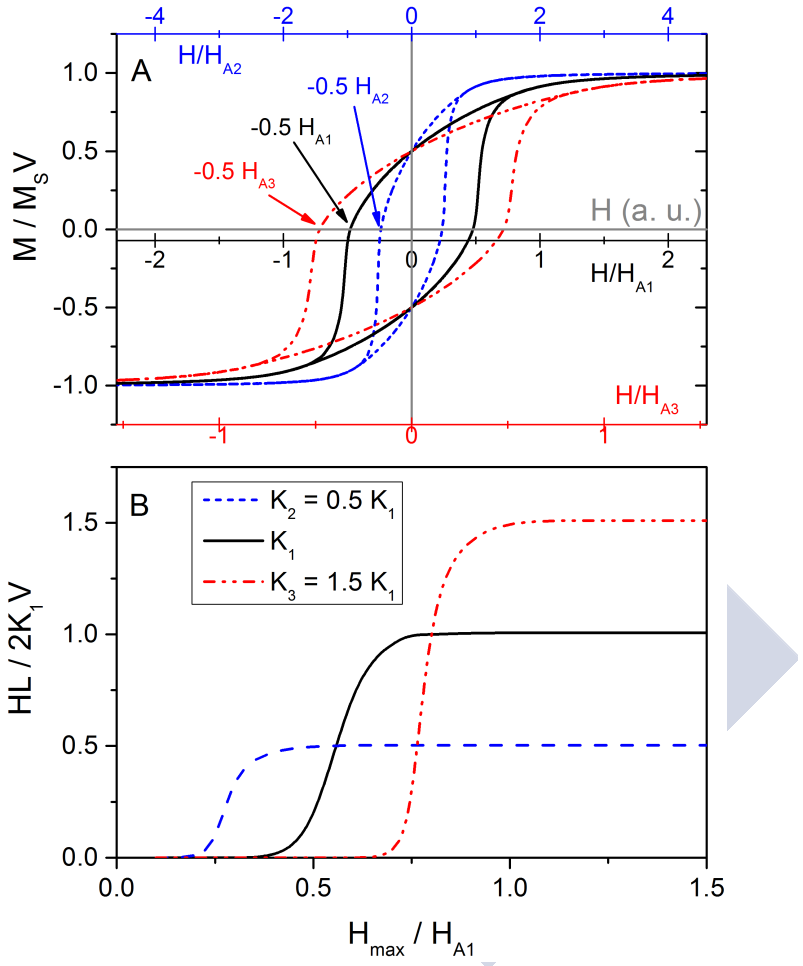

Figure 1.3: A: Hysteresis cycles for three samples with different anisotropy constant K. The additional x-axes illustrate how the coercive field for the Stoner-Wohlfarth model is recovered when considering the H/H_A scaling. B: Hysteresis losses as a function of the applied field for the samples of panel A. [This figure belongs to paper 2 in chapter 6.]

1.3.3 Simulation process

The process to perform the simulations consists in: 1) Allocating the particles in a regular lattice and relaxing the sample to a liquid-like distribution considering a Lennard-Jones potential. This gives the positions of the particles forming the frozen ferrofluid. 2) Assigning

features such as anisotropy, magnetization saturation and volume to the particles and selecting applied field and temperature conditions. The direction of easy-axes and the initial direction of the magnetic moments is also fixed. 3) Letting the system evolve under the magnetic field and given the energies mentioned in subsection 1.3.2. The magnetic moment progression is calculated with the Metropolis algorithm and saved together with the applied field to later calculate the hysteresis loop area. Both global and local magnetic moments and areas are obtained. Note that in these calculations, *local* refers to a particle belonging to a group of MNPs inside the sample having the same features (size, anisotropy). This way, local heat would be the quantity of thermal energy that the MNPs belonging to these subsets are able to release. The number of Monte Carlo steps was adjusted so the Stoner-Wohlfarth[20] coercive field $H_C \approx 0.48 H_A$ and remanence magnetization $M_R \approx 0.5 M_S V_t^0$ are recovered for a non-interacting ensemble of MNPs at very low temperature.

1.3.4 Metropolis algorithm

Metropolis algorithm[59] allows to calculate the evolution of the magnetization. It is based on a Markov chain model, which describes a sequence of a finite number of attainable events. The probability of the next event only depends on the current state of the system and not on the other previous events. Metropolis algorithm will randomly select one particle i from the sample, it will calculate its current energy $E_{current}$ and will generate a new possible state with energy E_{new}. In principle, the new state can be chosen at random. However, the code used for this work defines a cone of a few degrees delimiting the scope of the new possible state taking temperature into account. This is based on the Time Quantified Monte Carlo step model.[71,72] If $E_{new} \leq E_{current}$, the new state will be accepted. If the opposite occurs, the new state will be accepted with Boltzmann probability $P = e^{-(\Delta E / k_B T)}$, where $\Delta E = E_{new} - E_{current}$. A random number between 0 and 1 is generated and compared to the probability P. If P is greater than the random number, the new state is accepted. Otherwise, it is rejected. This process will be repeated N times, constituting one Monte Carlo step and being N the number of particles of the system. Then the average magnetic moment can be calculated by weighting all the configurations evenly. Selecting configurations with Boltzmann probability and then weighting them evenly is called *importance sampling*.[73,74] This is an advancement respect to previous Monte Carlo schemes, where the configurations were selected randomly and later weighted by Boltzmann probability (straightforward sampling). Importance sampling is the great advantage of the Metropolis algorithm because it allows to reduce the number of sampled configurations and allows to account only for configurations having non-vanishing weights.

USC
UNIVERSIDADE
DE SANTIAGO
DE COMPOSTELA

2 OBJECTIVES

The main objective of this thesis is the study of local (individual particle level) heating caused by size and anisotropy polydispersity and how it compares with the global one in the framework of MNH. This is motivated by: 1) the need to improve the control of the heating performance of MNPs, and 2) the aforementioned MNH experiments reporting cell death without a noticeable macroscopic temperature increase together with experiments showing very high temperature gradients decaying to zero just a few nanometers away from the particle surface. This thesis will focus on studying the following aspects and answering the associated questions:

2.1 Effect of size polydispersity

MNPs synthesis techniques are not able to produce perfect size monodisperse samples, that is to say, an ensemble of particles where all particles have the same size. Experimentally, a size dispersion lower than 10% is already considered as monodisperse. Given that dissipated energy is proportional to particle volume, each particle with different size will release a different amount of energy. Therefore, there will not be uniform heating in the treatment area but a collection of spots with a variety of heating performances. Possible associated local infra- and over-heating effects may be problematic for MNH efficacy and safety: On the one hand, if heating is not enough and cancer cells are not sufficiently damaged, the treatment would not be as effective as desired. On the other hand, if heat supply is excessive, surrounding healthy tissue may be injured and non-desired necrotic death paths may be activated.[6,18] There is an associated interesting consideration, which is that two particle systems may present the same SAR global values but completely different local heating behavior because of size polydispersity. Accordingly, it is crucial to know how size dispersion σ affects heating in MNH, not only globally, but especially at a local level. This is the first aim of this thesis and it is illustrated in Fig. 1.1. It is worth noting that there several theoretical[23,29,75–77] and experimental[62,66,67,78,79] works which have studied the influence of size polydispersity on MNH, but always from a global (entire system) perspective.

2.2 Using local heat to optimize average particle size

MNH efficacy is usually reported in terms of global SAR. It is believed that the higher the global SAR, the better for the MNH treatment. This is why many MNH research works study how to optimize MNPs parameters or the applied field amplitude and frequency to obtain a global SAR value as large as possible. However, as mentioned above, size polydispersity may cause different local heating performance which likely affects MNH effectiveness. This should be taken into account regarding MNH effectiveness and safety. The second objective of this thesis is to correlate local heat dissipation with expected MNH efficacy. In particular, the goal

is to develop a theoretical approach that indicates what is an adequate average particle size, taking into account common size dispersion values, that allows to have the greatest number of particles releasing energy in a desired SAR range. Fig. 2.1 illustrates this objective by showing two SAR distributions: one corresponding to a more polydisperse sample with a lower global SAR value and the other corresponding to a less polydisperse sample with a larger global SAR value. This scenario challenges the usually presumed idea that the higher the global SAR value, the better. In this particular case and assuming the desired SAR range marked in the figure, having a more polydisperse sample with a lower global SAR value would be preferable since more MNPs would be releasing energy in the target SAR range. SAR_{min} and SAR_{max} would indicate safety limits regarding local over- and infra-heating effects.

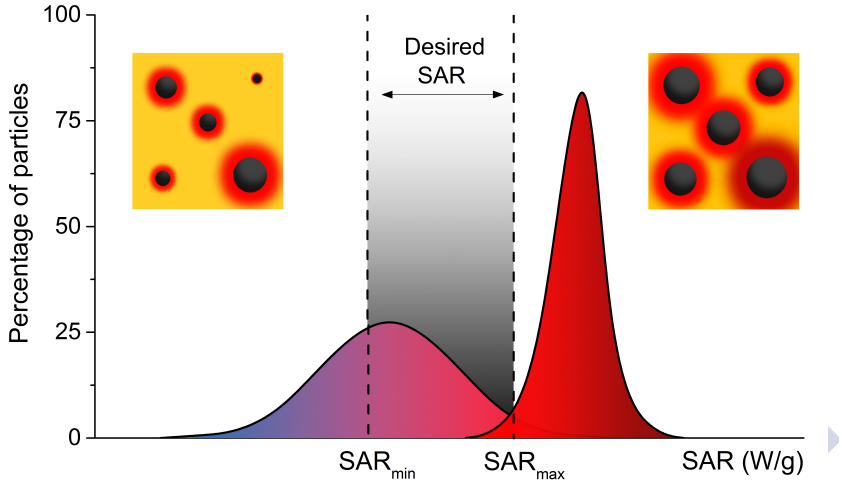

Figure 2.1: Scheme of two SAR distributions. One of them corresponds to a system with a low size dispersion and a high global SAR value. The other one corresponds to a system with a higher size polydispersity and a lower global SAR. The gray shadowed region represents the target SAR, where SAR_{min} and SAR_{max} would denote safety limits for avoiding local over- and infra-heating effects. [This figure can be found in the link of Ref. 80 as the graphical abstract of paper 2, see chapter 6.]

2.3 EFFECT OF ANISOTROPY POLYDISPERSITY AND APPLIED FIELD

Besides size, particle anisotropy K has a significant effect on the heating capabilities of MNPs. Firstly, energy dissipation is proportional to K, as it is also to particle volume. K determines the maximum achievable heating output, which is $\approx$ 2KV for a random non-interacting ensemble of MNPs. In addition, the relation between K and the amplitude of the applied field H_{max} determines if the hysteresis loop opens and therefore heat is released. These two aspects are clearly seen in Fig. 1.3B. For a non-interacting system with randomly distributed easy axes, heat dissipation is negligible until $H_{max} \approx 0.5H_A$,[81] being $H_A = 2K/M_S$ the anisotropy field.

As with size, a particle sample will present an unavoidable anisotropy distribution. The effect of anisotropy dispersion on MNH was studied in Ref. 12, but only from a global point of view. It is clear that it is necessary to study the effect of having an anisotropy distribution respect to local heating and also investigate the amplitude field effects. This is the third aim of this thesis, which Fig. 2.2 illustrates. The insets show that the anisotropy distribution can be linked to particle aspect ratio. Optimizing the choice of the anisotropy constant and the amplitude of the applied field to ensure an effective and safe MNH treatment will be an additional goal.

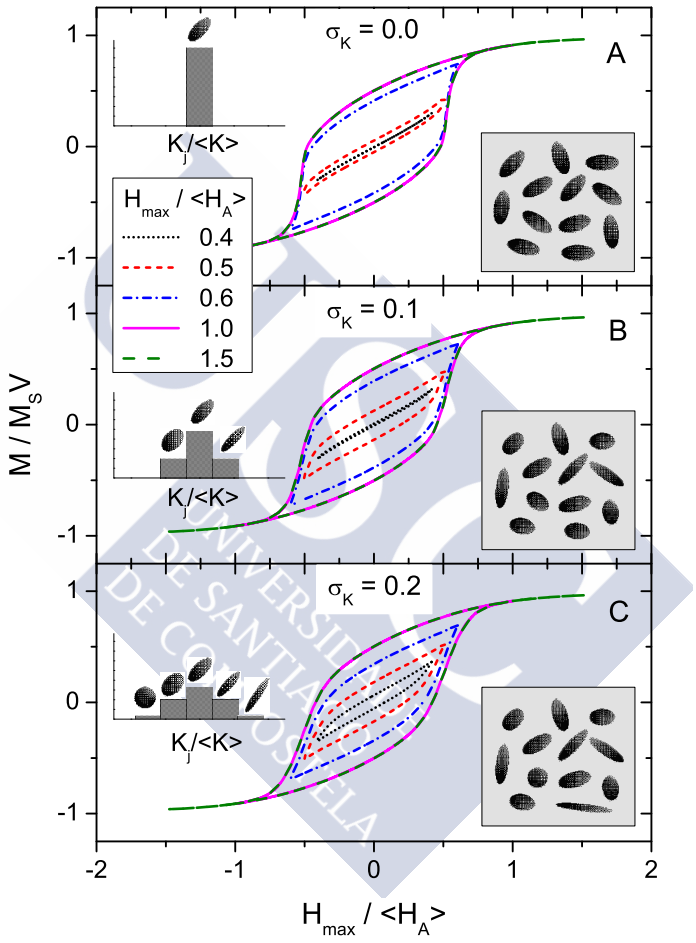

Figure 2.2: Global hysteresis cycles for various $H_{max}/\langle H_A\rangle$ values and three degrees of anisotropy dispersion σ_K. The insets show the possible associated systems and how the aspect ratio of the MNPs links with the anisotropy distributions. Here $\langle K\rangle = K_0$. [This figure belongs to paper 3 in chapter 7.]

USC
UNIVERSIDADE
DE SANTIAGO
DE COMPOSTELA

3 GENERAL DISCUSSION

This chapter describes the main results of this thesis according to the aims explained in chapter 2 and following the methodology detailed in section 1.3. The associated papers can be found in chapters 5, 6 and 7.

Since heat is proportional to volume V, correlating volume with the lognormal diameter distribution generally reported in experiments is important. If a variable x is lognormally distributed, the expected value of x^n is

$$E(x^n) = e^{\left\{nU+\frac{1}{2}n^2\sigma^2\right\}}. \tag{3.1}$$

In this case x corresponds to diameter D and n corresponds to 3 since $V \propto D^3$. U was defined in Eq. 1.8 as the average of the logarithms of the diameter: $U = \langle \ln D \rangle$. Therefore, Eq. 3.1 becomes $\langle V \rangle = e^{3U+\frac{9}{2}\sigma^2}$. In order to get an expression for U, Eq. 3.1 with n = 1 is used. This way, the average diameter is obtained as $\langle D \rangle = e^{\left\{U+\frac{1}{2}\sigma^2\right\}}$. Taking logarithms in both sides, U becomes: $U = \ln\langle d \rangle - \frac{1}{2}\sigma^2$. Thus, the effect of σ on average volume is given by

$$\langle V \rangle = e^{3\left(\ln\langle D \rangle+\sigma^2\right)}. \tag{3.2}$$

In normalized units (see subsection 1.3.2) Eq. 3.2 turns into $\langle v \rangle = e^{3\left(\ln\langle d \rangle+\sigma^2\right)}$, and since $\langle d \rangle = 1$, it is obtained:

$$\langle v \rangle = e^{3\sigma^2}. \tag{3.3}$$

Eq. 3.3 already anticipates an important aspect for MNH: systems with the same mean diameter but higher σ are more robust against thermal fluctuations. Several diameter lognormal distributions for the same average diameter and different size dispersions are depicted in Fig. 3.1, showing that $\langle v \rangle$ increases with σ for a fixed $\langle d \rangle$. The inset of Fig. 3.1 illustrates how Eq. 3.3 agrees with the $\langle v \rangle$ data used in the calculations of the first paper of this thesis in chapter 5.

The dependence of mean volume on size dispersion given by Eq. 3.3 is used to predict how σ affects the maximum achievable normalized global hysteresis losses for a non-interacting system HL_{max}. Recalling subsection 1.3.2, it can be written:

$$HL_{max}/HL^0_{max} = 2KV_t/2KV^0_t = V_t/NV_0 = \langle v \rangle = e^{3\sigma^2}. \tag{3.4}$$

This expression is valid at very low temperatures, for non-interacting conditions and applies to major loop conditions. The good agreement between the simulated normalized hysteresis losses at very low temperature $hl\,(\sigma)$ are consistent with Eq. 3.4 can be seen in the inset of Fig. 4 of paper 1 in chapter 5.

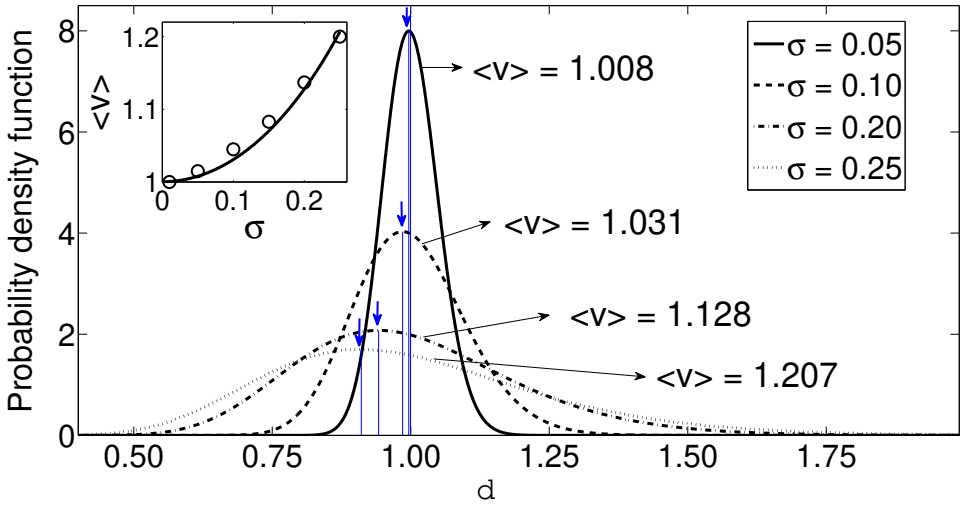

Figure 3.1: Lognormal distributions for systems keeping the same average diameter but having different size dispersion σ. The normalized average volume $\langle v \rangle$ is indicated for each distribution. The mode (most probable value) associated to each sample is marked with an arrow. The inset shows the $\langle v \rangle$ data used in the calculations of the first paper of this thesis in chapter 5 (open circles) and the analytical expression 3.3. [This figure belongs to paper 1 in chapter 5.]

The next step is knowing how size polydispersity affects local heat dispersion. The parameter used to quantify local heat dispersion is the standard deviation s_{hl}, which is defined as:

$$s_{hl} = \sqrt{\frac{1}{N}\sum_{j=1}^{P} N_j \left[(hl)_j - \langle (hl)_j \rangle\right]^2}. \tag{3.5}$$

Fig. 3.2 shows how much local heating deviates from the global one as a function of size dispersion σ and normalized temperature t, showing that s_{hl} rapidly increases with σ and decreases with temperature. The MNPs drawings illustrate that t can be linked to volume. Importantly, Fig. 3.2 implies that local heating dispersion can reach huge values. Fig. 3.2 also gives some insight about how particle size could be selected in order to limit local heat dispersion. Knowing the σ provided by a certain synthesis technique and the upper limit for s_{hl}, one could obtain particle volume for a given temperature. The horizontal line marked in Fig. 3.2 indicates that for keeping the same s_{hl}, a smaller particle size would be necessary if σ is higher. Accordingly, local heat dispersion would be decreased at the expense of getting less global dissipation. These two tendencies would need to be balanced in order to have an effective and safe MNH treatment.

The samples of MNPs used in MNH are concentrated. This means that interparticle interactions may play a significant role regarding heat dissipation and that they should be taken into account for more realistic predictions. Fig. 3.3 compares the global hysteresis losses as a

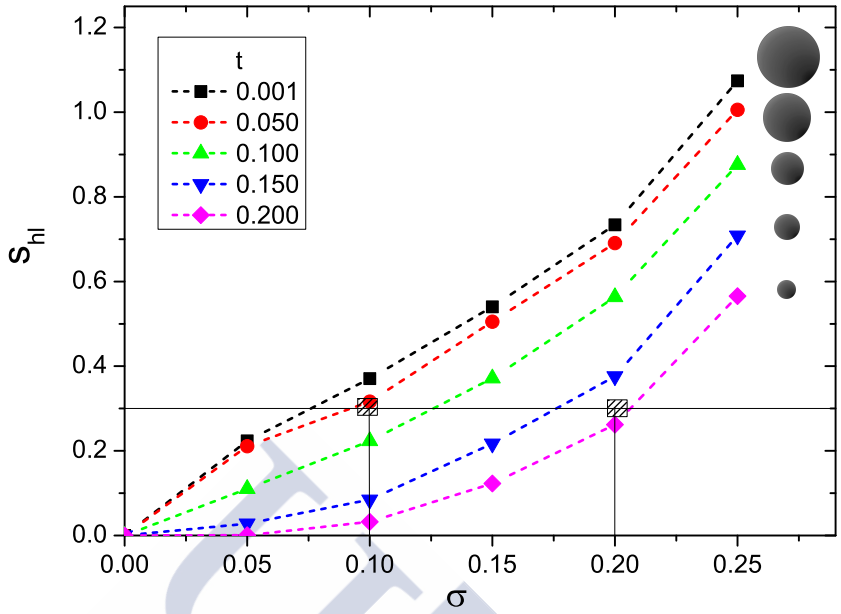

Figure 3.2: Standard deviation of the local hysteresis losses s_{hl} as a function of size polydispersity σ and for several normalized temperature t values. The drawings on the right indicate that increasing t is equivalent to decrease particle size. The horizontal and vertical lines illustrate two possible combinations of σ and t to avoid a local heat dispersion greater than 30%. [This figure belongs to paper 1 in chapter 5.]

function of size polydispersity for several temperature and particle interaction (volume fraction c) values. Fig. 3.3 shows that hl decreases with concentration at low temperature and that it increases with σ and c at high temperature. These findings agree with the results obtained in Refs. 29, 30, 70 and highlight the importance of considering interaction.

It is clear that size polydispersity, and therefore local heating performance, are crucial for MNH. Once this is known, the question of how to use this information to design a better MNH technique naturally follows. Then, the next step consists in analyzing how to choose average particle size depending on attainable size dispersion in order to have a more effective MNH. The premise is that efficacy increases if a greater number of MNPs are releasing energy in the desired SAR interval. The number of MNPs dissipating in a certain SAR range are calculated using the cumulative frequency. To give a realistic idea of the results, magnetite (Fe_3O_4) parameters and MNH field conditions are used. Fe_3O_4 is the most common and accepted material for MNH. The amplitude of the applied field was set to H_{max} = 500 Oe and the frequency to f = 500 kHz. Temperature was fixed to T = 300 K.

Different $\langle D \rangle$ values were considered to calculate the number of particles dissipating in SAR_j intervals of 50 W/g for two values of σ: 0.10 and 0.20. The results are depicted in Fig. 3.4. The black squares stand for the global SAR of the system for each average diameter case. Fig. 3.4 demonstrates that, depending on the desired SAR treatment scope, a different $\langle D \rangle$ will be preferable. Also, finding the most adequate average size is not necessarily related to

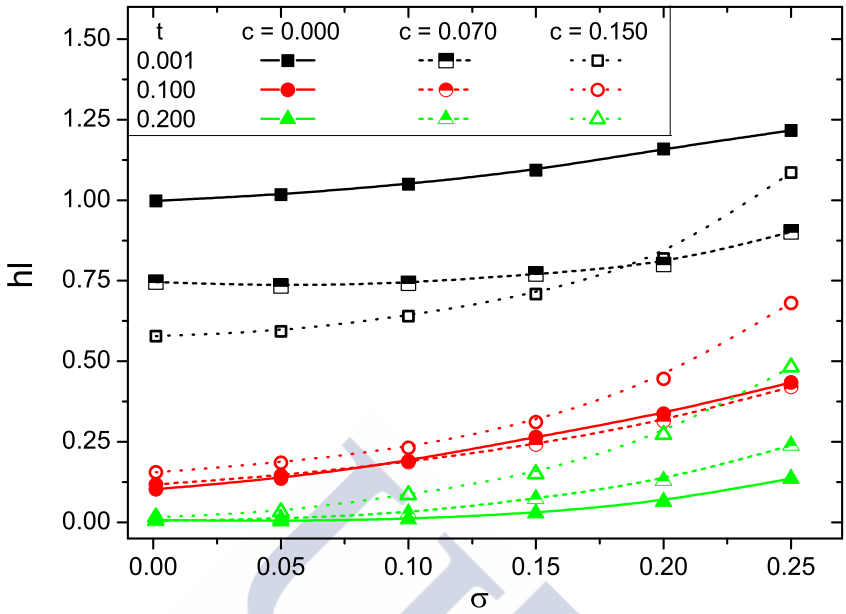

Figure 3.3: Normalized global hysteresis losses *hl* as a function of size dispersion σ. Different normalized temperatures t and concentration values c are considered. [This figure belongs to paper 1 in chapter 5.]

boosting global SAR since most of the MNPs might release energy in a different SAR interval. This result goes against the presumed need to enhance global SAR as much as possible and highlights once again the importance of considering local heat.

Until now the focus has been on analyzing the role of size polydispersity on the heating performance. However, as explained in subsection 1.1.1, the heating output of the MNPs is also defined by their anisotropy K. Taking into account the double role of anisotropy K as an indicator of the maximum achievable released energy and also considering that its relation with the applied field is key to enable heat dissipation, the effect of anisotropy dispersion σ_K on global and local heating is the following aspect to be examined.

The variation of the global hysteresis losses HL with field amplitude for three values of σ_K can be seen in Fig. 3.5A. Depending on the effect of $H_{max}/\langle H_A \rangle$ and σ_K, three regions can be distinguished. HL are larger for bigger σ_K if $H_{max} < 0.5\langle H_A \rangle$. The opposite occurs at $0.5\langle H_A \rangle < H_{max} < 1.0\langle H_A \rangle$. If $H_{max} > 1.0\langle H_A \rangle$, the anisotropy dispersion does not affect at global level. Fig. 3.5B explains these results by showing the anisotropy categories and the percentage of MNPs contributing to the released heat at the selected applied fields. Increasing σ_K allows MNPS with lower K_j and thus lower coercive field H_C to dissipate at smaller fields since H_{max} would be enough to open the loop. If the field is higher, increasing σ_K would reduce HL since the field would not be sufficiently high to open the cycles for the biggest K_j categories. Finally, if the field is big enough so every particle of the sample is in the blocked state, anisotropy polydispersity will not affect at a global level.

These results can explain, for instance, why $CoFe_2O_4$[82] and Fe_3O_4[83] MNPs give a rela-

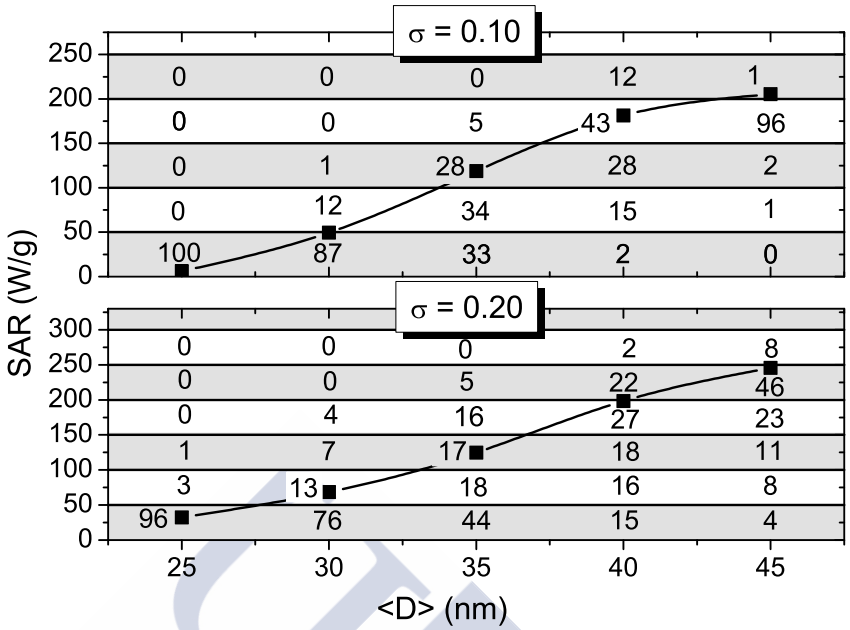

Figure 3.4: Percentage of Fe_3O_4 MNPs releasing energy inside SAR ranges of 50 W/g as a function of mean particle diameter $\langle D \rangle$. Two size dispersion values σ are considered. The black squares stand for the global SAR for each sample. [This figure belongs to paper 2 in chapter 6.]

tively low SAR value of ≈30 W/g despite having an anisotropy constant in the range of $10^5 J/m^3$ whereas $MnFe_2O_4$ MNPs[82] having a much smaller anisotropy constant of the order of $10^3 J/m^3$ give a SAR value of ≈170 W/g. Field amplitude is H_{max} = 200 Oe for all cases. Initially, one would expect the MNPs having the bigger k to have the higher SAR since SAR ∝ K,[21] but this is not the case. If the ratio H_{max}/H_A is analyzed, it is very close to 1 (≈0.9) for $MnFe_2O_4$ MNPs ($H_A \approx 220$ Oe) and less than 0.2 for $CoFe_2O_4$ and Fe_3O_4 MNPs ($H_A \approx 1300$ Oe). Thus Fig. 3.5 indicates that $MnFe_2O_4$ sample may be in major loop conditions (the majority of the particles would be releasing energy) and that the $CoFe_2O_4$ and Fe_3O_4 samples may be in minor loop conditions (just the MNPs with lower anisotropies would be dissipating).

Again, a question regarding the effect of σ_K and H_{max} on local heat dispersion arises. Similarly to size, standard deviation σ_{HL} was used to compute how much local dissipation deviates from the global one for different applied fields:

$$\sigma_{HL} = \sqrt{\frac{1}{N}\sum_{j=1}^{P} N_j \left(\frac{HL_j}{2\langle K \rangle V} - \frac{HL}{2\langle K \rangle V} \right)^2}. \tag{3.6}$$

This information is illustrated in Fig. 3.6 (left axis) for $\sigma_K = 0.20$. The right axis of Fig. 3.6 shows the standard deviation, but normalized to global released energy. This takes into account that the magnitude of the heat dispersion is linked to an average value, illustrating that it is not the same to have 5 ± 3 than 1 ± 3. At low fields σ_{HL} is small, but since global dissipated

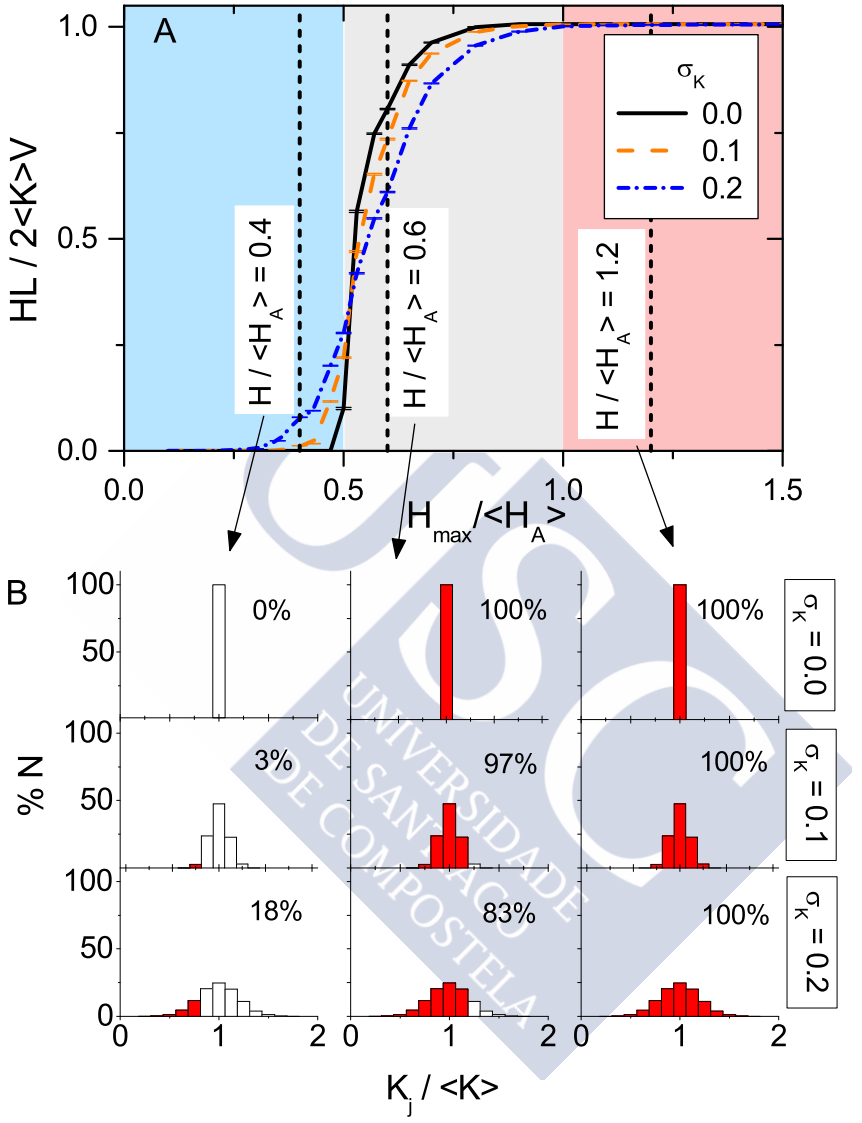

Figure 3.5: A: Normalized global hysteresis losses as a function of normalized applied field $H_{max}/\langle H_A\rangle$ for three anisotropy dispersions σ_K. Three field regions are differentiated. B: Anisotropy distributions for the three field values marked in panel A and three σ_K values. The colored bars stand for the anisotropy categories contributing to energy release. The numbers indicate the percentage of particles dissipating heat for each $(H_{max}/\langle H_A\rangle, \sigma_K)$ case. [This figure belongs to paper 3 in chapter 7.]

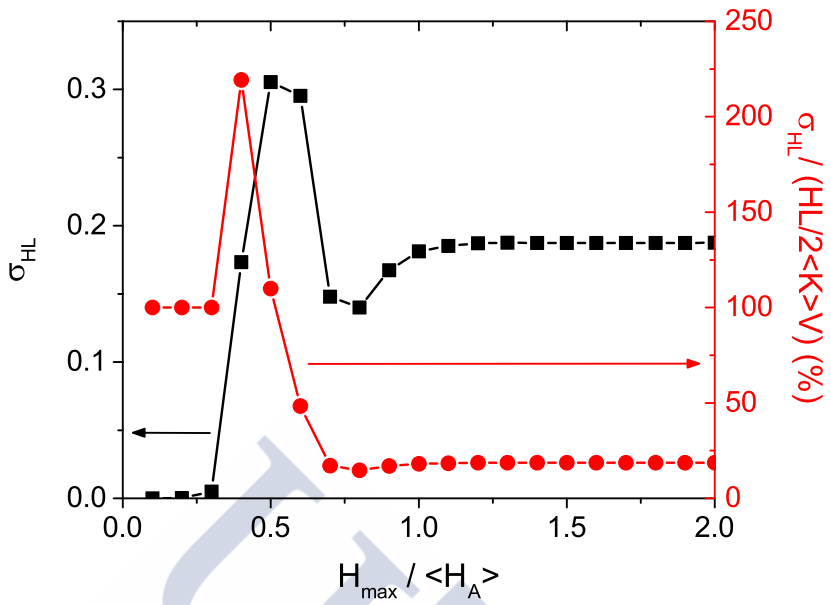

Figure 3.6: Evolution of the local heat dispersion σ_{HL} with the applied field (left axis). σ_{HL} normalized to the global heat dissipation expressed and expressed in percentage. [This figure belongs to paper 3 in chapter 7.]

energy is small as well, heat dispersion becomes significant. The contrary happens at high fields: standard deviation is big and global heat released too, so heat dispersion is not that much important in this case. This indicates that having major loop conditions would be convenient for achieving homogeneous local heating. If the applied field cannot the increased to ensure this condition, MNPS with lower anisotropy would help to decrease local heat dispersion.

USC
UNIVERSIDADE
DE SANTIAGO
DE COMPOSTELA

4 CONCLUSIONS

This thesis has studied the influence of size and anisotropy dispersion in MNH, both from a global entire system but especially from a local individual particle perspective. The main conclusions extracted are:

1. Even a low size or anisotropy polydispersity can greatly affect local heat dissipation, creating a broad distribution of local heating spots. This constitutes a challenge for designing an efficient and safe MNH treatment because some treatment areas may be over-heated while others may be infra-heated.

2. The need to differentiate between global heating and MNH efficacy is demonstrated. Achieving high global SAR values does not necessarily imply having a more effective MNH treatment.

3. Local heat dispersion, which was quantized with the standard deviation, can be very high, reaching or even overcoming the 100%. For size polydispersity, temperature or size have proved to be relevant parameters to consider. For anisotropy polydispersity, the amplitude of the applied field is a key feature.

4. Using dimensionless units may be useful to find an appropriate average particle size which, for an achievable size polydispersity depending on the synthesis technique, limits the local heat dispersion. This is mainly done by reducing particle size, which also decreases heating output. Therefore, both effects should be balanced in order to have both a safe and effective MNH treatment.

5. A theoretical approach on how to choose the most adequate average particle size according to an attainable size dispersion in order to have as much as MNPs as possible dissipating in the desired SAR range has been presented.

6. Three field regimes are differentiated considering the interplay of σ_K and $H_{max}/\langle H_A \rangle$: If $H_{max} < 0.5\langle H_A \rangle$, increasing σ_K will allow for more energy dissipation because the MNPs with smaller K will have a coercive field lower than H_{max}. On the contrary, decreasing σ_K will enable more released energy if $0.5\langle H_A \rangle H_{max} < 1.0\langle H_A \rangle$ since the applied field will not be enough to open the hysteresis cycle for the MNPs with higher anisotropy. Finally, if the applied field is big enough to make every particle in the sample to dissipate, $H_{max} > 1.0\langle H_A \rangle$, the effect of changing σ_K will just be noticeable at a local level.

7. In order to achieve homogeneous local heating, major loop conditions are prefered. If there are upper constraints in the amplitude of the applied field, choosing MNPs with low anisotropy may be advisable.

USC
UNIVERSIDADE
DE SANTIAGO
DE COMPOSTELA

The role of size polydispersity in magnetic fluid hyperthermia: average vs. local infra/over-heating effects

C. Munoz-Menendez, I. Conde-Leboran, D. Baldomir, O. Chubykalo-Fesenko and D. Serantes

Phys. Chem. Chem. Phys., 2015, **17**, 27812
DOI: 10.1039/C5CP04539H

USC
UNIVERSIDADE
DE SANTIAGO
DE COMPOSTELA

Distinguishing between heating power and hyperthermic cell-treatment efficacy in magnetic fluid hyperthermia

C. Munoz-Menendez, I. Conde-Leboran, D. Serantes, R. Chantrell, O. Chubykalo-Fesenko and D. Baldomir

Soft Matter, 2016, **12**, 8815
DOI: 10.1039/C6SM01910B

USC
UNIVERSIDADE
DE SANTIAGO
DE COMPOSTELA

Towards improved magnetic fluid hyperthermia: major-loops to diminish variations in local heating

C. Munoz-Menendez, D . Serantes, J. M. Ruso and D. Baldomir

Phys. Chem. Chem. Phys., 2017, **19**, 14257
DOI: 10.1039/C7CP01442B

USC
UNIVERSIDADE
DE SANTIAGO
DE COMPOSTELA

FURTHER WORK

After finishing paper 1, (see chapter 5) and while using the Metropolis Monte Carlo code to further study the effect of interactions at local level, an unexpected peculiarity appeared: some local hysteresis loops for the smaller particles were inverted, that is to say, they had negative remanence. This feature is shown in Fig. 7.1. Whereas the global hysteresis loop in the left panel follows the common counterclockwise direction, this is not the case for all the local cycles when the different size categories are analyzed. The right panel illustrates how one of the local loops is traversed clockwise instead of counterclockwise as usual.

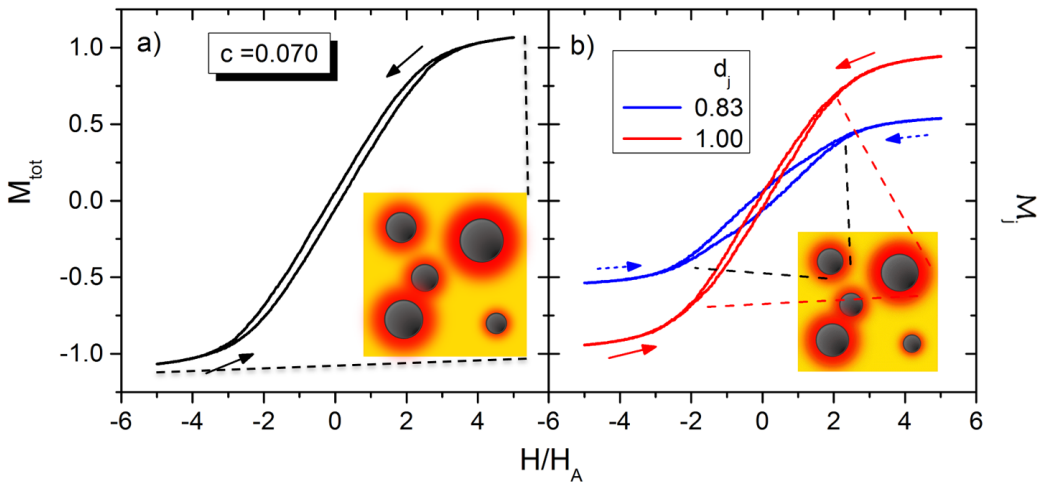

Figure 7.1: Left panel: global hysteresis loop for a size polydisperse sample with $c = 0.070$. Right panel: hysteresis cycles for two size categories of the sample. The one with $d_j = 0.83$ is inverted, that is to say, shows negative remanence.

The emergence of these inverted loops can be understood when considering that the interparticle dipolar field H_D can greatly modify the local field felt by the particles. For simplicity, let us consider the case where the MNPs have uniaxial anisotropy and the magnetic field is applied in the z-direction $\vec{H} = H\hat{z}$, parallel to the easy axes of the MNPs. In a non-interacting situation, the magnetization will switch when the condition $H > H_A$ is fulfilled, where H_A is the anisotropy field. If interaction is present, the magnetization will reverse for the condition $H > H_A + H_D$. H_D can take both positive and negative values depending on the relative orientation of the MNPs. This can be seen in Fig. 7.2. In the left side of Fig. 7.2, H_D and H_A have the same sign, so the resulting interacting hysteresis cycle is wider then the non-interacting one. However, when H_D and H_A have opposite signs as in Fig. 7.2b), the interacting loop is narrower than the non-

interacting one. Accordingly, it is easy to see that if H_A and H_D have opposite signs and the magnitude of H_D is bigger than the magnitude of H_A, magnetization switching will take place at positive values of the applied field H. Thus, an inverted loop with negative remanence as the one shown in Fig. 7.1b) is obtained. The emergence of local inverted cycles may seem surprising at first, but as it has been shown, they are a natural consequence of the reversing condition $H > H_A + H_D$.

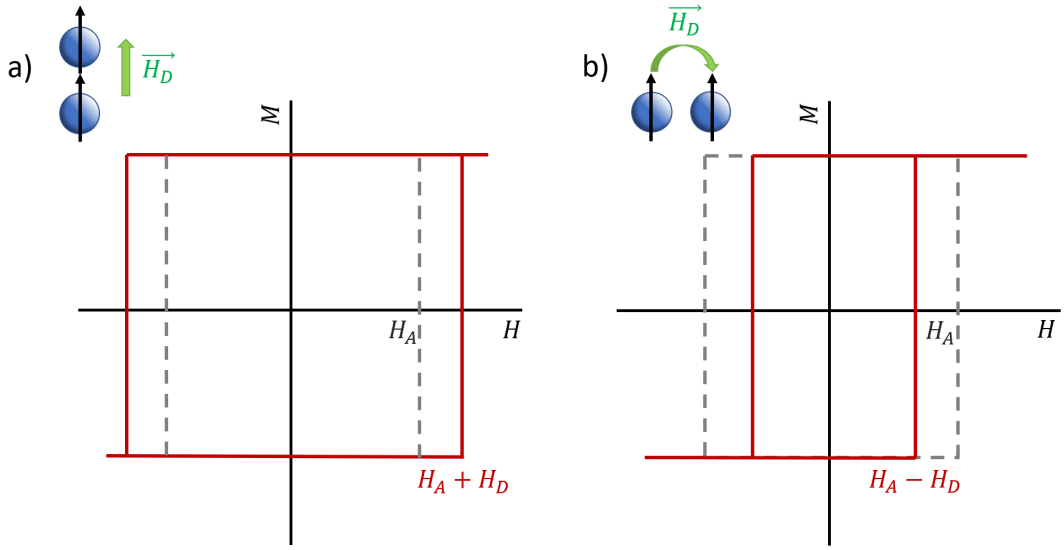

Figure 7.2: Hysteresis loops for the two different MNPs orientations illustrated. The gray dashed cycle stands for the non-interacting case, which act as a reference. The full lines represent the interacting cases: a) The particles are aligned along the z-axis. b) The particles are aligned perpendicularly to the z-axis.

The immediate questions that arise after seeing this initially unexpected behavior are: what implications do these inverted local hysteresis loop have for MNH? Can the area of these loops quantify local heat? Is a negative local area indicating heat absorption instead of heat dissipation? These aspects are crucial and have significant consequences for HMN that need clarification. Answering these questions is complex and the search for explanations led to several national and international collaborations which will be outlined. Before starting to investigate these issues *per se*, Prof. Chantrell, in the University of York, U.K., is contacted. Prof. Chantrell is a world renowned researcher in the field of computational magnetism for being one of the main developers of multiscale, atomistic and Monte Carlo models to study magnetic materials and nanoparticles. He has developed a kinetic Monte Carlo (kMC) technique[84] which allows to consider real time steps and proper dynamics for an interacting system. With this method, which has been applied to the aforementioned problem, local hysteresis cycles are also found. In addition, the results from energy minimization using analytical expressions obtained by Dr. Livesey, from the University of Colorado Colorado Springs, U.S., reproduce the computational observations from Metropolis and kinetic Monte Carlo techniques too.

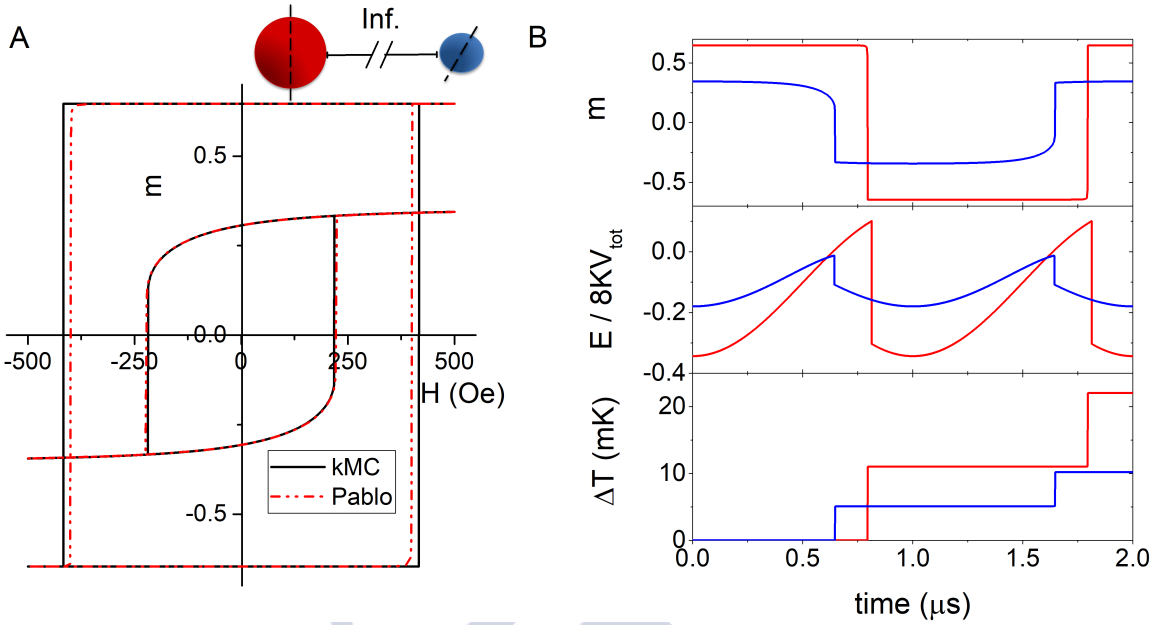

Figure 7.3: Comparison between kMC and LLB-LC simulations for the non-interacting case. Two particles with the same K and M_S but different size are considered. One has a diameter of 22 nm and the other one of 18 nm. The easy axis of the big particle lies in the z-direction and the easy axis of the small particle is tilted 30 ° from the z-axis. The field is applied in the z-direction. A: Local hysteresis loops. B, from top to bottom: magnetization, total energy and temperature evolution along a hysteresis cycle for each particle.

Once that the existence of local inverted loops has been ratified, one can think about their meaning. Is it possible that the area of a local inverted cycle stands for heat absorption? There are works showing negative remanence[85,86], developing models for clockwise hysteresis[87] or reporting both positive and negative values in a work distribution[88], but a thermodynamic interpretation for negative hysteresis is lacking. Ref. 85 interprets that during an inverted loop, both heat dissipation and absorption take place in such a way that at the end only energy released remains. How can inverted cycles reconcile with thermodynamics? Without the need to solve this issue at first, an initial response to the question whether the area of a local inverted loop is absorbed heat can be provided, being the answer *no*. The associated reasoning is that if a particle feels a certain local field, this will make the magnetization of the particle switch and release energy no matter the origin of the different contributions to that local field. This argumentation should be proved mathematically, but an appropriate thermodynamic framework to do so is lacking. In order to help with this part, Dr. Hovorka, from the University of Southampton, U.K., was contacted. The preliminary results using non-equilibrium thermodynamics supports the idea that the area of a local cycle with negative remanence is not absorbed heat.
In view of this, how can local heat be quantified with the available techniques? Since the evolution of the magnetization depends on the energies of the particles, a strategy of tracking and analyzing individual particle energy as a way to quantify local energy dissipation is imple-

mented with the kMC. Interestingly, kMC predicts that the non-switching particle can release energy and that there are three different types of energy processes regarding local dissipation. However, the analysis of different interaction conditions shows that the energy variation alone is not enough to calculate local heat dissipation in interacting systems. To work out this issue, a collaboration with Dr. Chubykalo-Fesenko from the Instituto de Ciencia de Materiales de Madrid, Spain, and Dr. Nieves from Universidad de Burgos, Spain is established in order to use a Landau-Lifshitz-Bloch - Lattice Coupled (LLB-LC) technique.[89,90] LLB-LC simulates the magnetization and phonon temperature dynamics of ferromagnets in a self-consistent way using a Landau-Lifshitz-Bloch equation. This method is the first one in considering the effect of magnetization on temperature and directly provides particle temperature. Interestingly, this technique shows that MNPs always dissipate heat and that in certain cases a particle whose magnetic moment does not switch can release more energy that a switching neighboring particle. An illustrative example showing the comparison between kMC and LLB-LC for two non-interacting MNPs is depicted in Fig. 7.3.

Fig. 7.3A demonstrates that the results of both techniques are comparable since the hysteresis loops of each particle agree for kMC and LLB-LC. Fig. 7.3B shows that kMC predicts an energy drop ΔE and LLB-LC predicts a temperature increase ΔT when the magnetization of one of the MNPs reverses. When converting to the same units, the sum of the ΔE agrees with the sum of the ΔT for each particle. The global area of the system can be recovered from both energy and temperature variation.

A manuscript reporting the above novel results is currently under preparation. Future work will try to use the findings from the LLB-LC approach as a guide to obtain the local heat in terms of the energies involved in the kMC technique. Since the LLB-LC method is highly computationally demanding, being only suitable to study small systems up to microseconds, the envisaged future work would allow to calculate local heat correctly in big systems of MNPs and to achieve experimental timescales.

RESUMO

As nanopartículas magnéticas (NPMs) disipan calor cando son sometidas a un campo magnético alterno. Esta calor que liberan na nanoescala ten usos potenciais nun amplo rango de campos tecnolóxicos, dende catálise ata nanomedicina. Esta tese trata con algúns aspectos pouco estudados da hipertermia magnética con nanopartículas (HMN), un novo e prometedor tratamento médico que ten como obxectivo destruír as células cancerosas. Isto conséguese introducindo NPMs na área a tratar e quentándoas ao aplicar un campo magnético alterno dende o exterior. Idealmente, a temperatura do tumor estaría entre os 43 e os 45°C. Esta técnica baséase en que as células cancerosas son máis sensibles a un aumento de temperatura que as células sans e en que a amplitude e a frecuencia do campo aplicado non son prexudiciais para o corpo humano. A HMN ten unha vantaxe moi grande respecto aos tratamentos convencionais para o cancro, como son a quimioterapia ou radioterapia, e é que é unha técnica localizada. Ao introducir as NPMs unicamente na zona a tratar, evítanse efectos secundarios en todo o corpo non desexados e o tecido san non sofre danos.

Para levar a cabo unha HMN tanto efectiva como segura, é importante escoller as NPMs e o campo aplicado con características axeitadas. En primeiro lugar, as NPMs deben ser biocompatibles, non tóxicas a estables. A maiores, hai que ter en conta que certas propiedades das NPMs son especialmente relevantes. O tamaño das NPMs afecta a como entran nas células, á tendencia que teñen de agregarse e á súa capacidade de quecemento. A forma e a relación de aspecto tamén inflúen na incorporación das NPMs ás células e ao quecemento. A maiores, a forma e a relación de aspecto determinan a anisotropía efectiva das NPMs. Estes aspectos son cruciais xa que a enerxía que as NPMs poden liberar é proporcional ao seu volume V e á súa constante de anisotropía K: $E \propto KV$. A anisotropía é moi importante, porque non só determina a enerxía máxima que as NPMs poden liberar, senón que tamén afecta á amplitude do campo necesaria para que comece a haber disipación de enerxía. Outro aspecto significativo é a homoxeneidade do sistema. Se as NPMs teñen diferentes características, a súa reacción fronte a un mesmo estímulo externo podería ser moi distinta. Isto podería provocar un quecemento dispar no sistema de NPMs considerado e é a premisa na que se basea esta tese. Por último a concentración das NPMs é imporante xa que regula a interacción dipolar entre as partículas do sistema e pode provocar respostas moi variadas en canto á disipación de calor.

A HMN recibiu a aprobación reguladora europea en 2013 e actualmente este tratamento está dispoñible en varios hospitais de Alemania. Ao longo de hai máis dunha década leváronse a cabo varios ensaios clínicos para diferentes tipos de tumores, como o de cerebro ou o de páncreas. Na actualidade séguense facendo máis ensaios clínicos.

A pesar do potencial e as vantaxes que presenta a HMN fronte a tratamentos convencionais, esta aínda non se utiliza de forma ampla a nivel clínico. Un aspecto a ter en conta é que o comportamento das NPMs cambia dependendo no medio no que estean dispersas. Así, non é o mesmo

estudar o comportamento e optimizar os parámetros das MNPs *in vitro* que o que pasará despois *in vivo*. Ademais, as NPMs tenden a degradarse nun entorno biolóxico e consecuentemente as súas propiedades en canto ao quecemento vense alteradas. No que se refire á física, o problema principal é o control preciso da enerxía que disipan as NMPs. Isto ten efectos relevantes na eficacia e na seguridade da HMN. Dunha banda, se o quecemento é excesivo, as células sans poden ser danadas. Doutra banda, se se quenta menos do necesario, o tecido tumoral non se verá suficientemente afectado e a HMN non será efectiva.

Nesta liña de conseguir un tratamento eficaz e seguro, no campo de investigación da MNH acostuma asumirse que é vital maximizar o quecemento das NPMs e acadar unha temperatura uniforme no tumor. Deste xeito, a dose de material magnético que se lle subministra ao paciente é menor e destrúense as células tumorais sen danar o tecido san respectivamente. Sen embargo, hai dúas cuestións que invitan a plantexarse o alcance destas ideas xeralmente aceptadas. A primeira é que as técnicas de síntese non son capaces de producir NPMs totalmente monodispersas en tamaño e forma. Entón, cada partícula disipará unha enerxía proporcional á súa anisotropía K e ao seu volume V. E se estes parámetros varían entre partículas, haberá distintos focos de calor *local*, a nivel de partícula, que poderán causar efectos de infra ou sobrequecemento coas consecuencias previamente mencionadas. A maiores, hai varios experimentos de HMN que informan de morte celular sen medir un aumento apreciable de temperatura *global*, é dicir, a nivel macroscópico. A pregunta que surxe é cal é a orixe destes resultados. Unha opción é que o dano nas células se deba a efectos mecánicos. Outra posibilidade é que a calor local sexa a causa. Esta última idea vese apoiada por outros experimentos que miden aumentos de temperatura na superficie das NPMs que acadan 70 $\circ$C por enriba da temperatura global. Estes gradientes de temperatura caen a cero a uns poucos nanómetros da superficie das partículas. Consecuentemente, queda claro que é importante e necesario estudar a calor local no marco da HMN.

Tendo en conta a necesidade de controlar a calor que disipan as NPMs e os experimentos mencionados no parágrafo anterior, esta tese céntrase en estudar os efectos que teñen na calor local a polidispersidade en K e en V e como isto se relaciona coa calor global. Todo iso analízase considerando as implicacións na efectividade e na seguridade da HMN e propóñense formas de mellorar estes dous aspectos.

Para investigar os efectos da calor local en HMN, fanse simulacións computacionais. A modelización non só permite entender os resultados experimentais e optimizar as características das NPMs, senón tamén axilizar a transferencia da nanomedicina do laboratorio ao hospital. Os cálculos necesarios fanse nun espazo tridimensional e para un número elevado de NPMs, o que require unha técnica de simulación axeitada para problemas complexos e de alta dimensionalidade. Polo tanto, nesta tese utilízase unha técnica de Monte Carlo cun algoritmo de Metrópolis para simular a evolución da magnetización fronte a un campo aplicado externo H e calcular a área HL do ciclo de histérese resultante. A magnitude que se usa habitualmente para informar das capacidades de quecemento en HMN é o SAR, siglas en inglés de *Specific Absorption Rate*. O SAR defínese como a taxa á que a enerxía electromagnética é absorbida por unha unidade de material magnético e ten unidades de W/kg. O SAR pódese obter multiplicando a área do ciclo de histérese pola frecuencia f do campo aplicado: $SAR = HL \cdot f$. Asúmese que este valor teórico

coincide co SAR que se calcula a partir da pendente inicial da curva de quecemento medida en condicións adiabáticas.

Considérase un modelo físico onde hai N NPMs monodominio cuxos momentos atómicos rotan coherentemente. Así, seguindo a aproximación de macroespín, cada partícula i pode ser descrita por un supermomento $\mu_i = M_{S_i} V_i$, sendo M_S a magnetización de saturación e V o volume. As NPMs teñen anisotropía uniaxial efectiva e os eixos fáciles distribuídos aleatoriamente. Seguindo varios experimentos que informan de que a contribución da relaxación Browniana á calor disipada é desprezable se as NPMs están en medio celular, as partículas están fixas nas súas posicións e non se consideran efectos de rotación das NPMs. Deste xeito, a única causa de disipación de enerxía é que os supermomentos salten por enriba da barreira de enerxía. A enerxía total do sistema ten tres contribucións: a enerxía de anisotropía, a de Zeeman (campo aplicado) e a dipolar (interacción entre partículas). Para tratar a polidispersidade, sexa en tamaño ou forma, créanse categorías. A cada categoría j asígnaselle un número de partículas N_j co mesmo diámetro ou anisotropía. Baseándose en traballos previos, o diámetro das NPMs segue unha distribución lognormal e a anisotropía unha distribución normal. Para distinguir entre os efectos de cada tipo de polidispersidade, fanse simulacións independentes de cada unha delas. Por xeneralidade, nesta tese trabállase con parámetros adimensionais. Isto permite interpretar os resultados en función de distintos materiais (K e M_S), tamaños, temperaturas e amplitude do campo aplicado. Así, o diámetro D e a anisotropía K de sistemas polidispersos normalízanse polos valores do sistema ideal monodisperso D_0 e K_0 respectivamente. O diámetro e a anisotropía promedio dos sistemas polidispersos mantense igual a estes valores D_0 e K_0. O campo aplicado $H0$ normalízase polo campo de anisotropía H_A e a enerxía térmica $k_B T$ divídese por $2KV_0$, onde k_B é a constante de Boltzmann, T é a temperatura e V_0 é o volume dunha partícula do sistema ideal monodisperso. Finalmente, a área dos ciclos de histérese normalízase pola enerxía máxima que un conxunto monodisperso de NPMs non interactuantes cos eixos fáciles distribuídos aleatoriamente pode acadar seguindo o modelo de Stoner-Wohlfarth: $HL^0_{max} = 2KV^0_t$, onde V^0_t é o volume total do sistema monodisperso, é dicir $V^0_t = NV_0$. As simulacións reproducen o re-escalado das perdas de histérese co volume e coa anisotropía.

O proceso de simulación ten varias etapas. Primeiro colócanse as partículas nunha rede regular para logo relaxar a estrutura ata ter unha distribución tipo líquido usando un potencial de Lennard-Jones. Despois, a cada partícula asígnanselle as súas características (M_S, K, V) e fíxase a amplitude máxima do campo aplicado, a temperatura, a dirección dos eixos fáciles e a dirección inicial dos supermomentos. A continuación déixase que o sistema evolucione baixo o campo aplicado e seguindo as enerxías previamente mencionadas. Gárdase a información da magnetización e o campo aplicado, tanto global como local, para posteriormente calcular a área dos ciclos de histérese. A variación da magnetización obtense co algoritmo de Metrópolis, que está baseado nun modelo de cadea de Markov. Isto implica que a probabilidade do seguinte suceso só depende do estado anterior e non do que pasara anteriormente. Este algoritmo escolle unha partícula do sistema ao azar, calcula a súa enerxía actual e xera un novo estado posible. O novo estado escóllese dentro dun cono ao redor do supermomento actual que ten en conta a temperatura. Se o estado novo ten unha enerxía menor que o actual, é aceptado. Se non a ten, será aceptado cunha probabilidade de Boltzmann $P = e^{-(\Delta E/k_B T)}$. Xérase un número aleatorio

entre 0 e 1. Se P é maior que o número aleatorio, pásase ao novo estado. Se non é o caso, o novo estado rexéitase. Este proceso repítese tantas veces como número de partículas teña o sistema ata completar un paso de Monte Carlo. O número de pasos de Monte Carlo axústase de tal xeito que se recuperen os valores do campo coercitivo e da remanencia do modelo de Stoner-Wohlfarth, $H_C \approx 0{,}48 H_A$ e $M_R \approx 0{,}5 M_S V_t^0$.

Esta tese divídese en tres obxectivos encadrados no estudo da calor local e como contrasta coa calor global no marco da HMN , onde cada un deles ten un artigo publicado asociado. O primeiro é estudar os efectos da polidispersidade en tamaño. Unha vez feito isto, o seguinte paso é correlacionar a calor local coa eficacia da HMN. En concreto, a meta é desenvolver unha aproximación teórica que indique cal é o tamaño promedio máis adecuado das MNPs para que o maior número posible delas estean disipando nos valores de enerxía de interese. Por último, investígase o efecto da polidispersidade en anisotropía e como afecta a amplitude do campo aplicado. A continuación faise unha discusión xeral dos resultados máis relevantes que se obtiveron ao ir cumprindo os diversos obxectivos.

No que se refire á polidispersidade en tamaño, é importante correlacionar o volume V coa distribución lognormal en diámetros xa que a calor disipada é proporcional a V. Isto faise utilizando o valor esperado da variable x^n, que se expresa mediante o momento de orde n. Neste caso úsanse os momentos de orde 1 (expresión para o diámetro promedio $\langle D \rangle$) e de orde 3 (expresión para o volume promedio $\langle V \rangle$) para expresar $\langle V \rangle$ en función da polidispersidade en tamaño σ para un mesmo $\langle D \rangle$. Esta relación aplícase para predicir analiticamente como σ afecta ás perdas máximas que un sistema non interactuante a moi baixa temperatura pode acadar. Os datos das simulacións coinciden cos valores que dan ambas ecuacións. A continuación estúdase a calor global e local en función da temperatura T e σ para finalmente calcular a dispersión en calor local empregando a desviación estándar s_{hl}. É notable que para unha baixa polidispersidade en tamaño, s_{hl} pode alcanzar valores moi grandes. Estúdase o papel que teñen T e σ en s_{hl} (s_{hl} aumenta rapidamente con σ e diminúe coa temperatura), e discútese como σ e s_{hl} se poden utilizar como guía para escoller un tamaño de partícula que limite a dispersión en calor local. Isto é posible grazas a traballar en unidades normalizadas. Posto que as mostras de NPMs en HMN son concentradas e a concentración regula a forza entre as NPMs, é importante entender que papel xoga este parámetro en HMN. Analízanse os efectos combinados da concentración, a polidispersidade en tamaño e a temperatura.

Unha vez analizada a influenza da polidispersidade en tamaño, a seguinte cuestión a responder é como utilizala para deseñar unha mellor técnica de HMN. Deste modo, estúdase como escoller o diámetro promedio do sistema en función do grao de dispersión σ para maximizar o número de partículas que estean liberando enerxía nun certo rango de SAR. A idea detrás disto é maximizar a disipación no intervalo de interese e minimizar os efectos de sobre e infraquecemento. Para calcular a cantidade de NPMs que liberan enerxía no rango de interese utilízase a frecuencia acumulada. E para dar un exemplo realista, os resultados danse para a magnetita Fe_3O_4, o óxido de ferro máis común e aceptado para HMN, e para unhas condicións de campo aplicado tamén usuais en HMN. Demóstrase que dependendo do SAR que se queira alcanzar e da polidispersidade en tamaño, un diámetro promedio ou outro será preferible. Tamén, que o diámetro promedio máis axeitado non é necesariamente o que proporciona un SAR global como

o que interesa nin tampouco un SAR maior. Isto débese a que, posto que hai unha distribución de SAR en función dos tamaños de partícula da mostra, parte das NPMs liberarán enerxía nun intervalo de SAR que non coincide co SAR global. Este resultado é significativo dado que vai en contra da idea de aumentar o SAR global o máximo posible que sempre se asume como correcta e adecuada.

Como se mencionou anteriormente, a calor liberada polas NPMs non só depende do seu volume senón tamén da súa anisotropía K. Tendo en conta o dobre papel que xoga K, dunha banda como parámetro chave na disipación máxima que se pode conseguir e doutra como regulador do campo aplicado necesario para que comece a disipación, analízase o efecto da dispersión en anisotropía σ_K tanto a nivel global como local. Diferéncianse tres réximes de campo en función dos valores de σ_K e da amplitude de campo H_{max} en relación co campo de anisotropía da mostra $\langle H_A \rangle$. Se $H_{max} < 0{,}5 \langle H_A \rangle$, aumentar σ_K permite liberar máis enerxía porque as NPMs con K menor teñen un campo coercitivo menor que H_{max} e abrirán o seu ciclo de histérese. Pola contra, para conseguir maior disipación no rango $0{,}5 \langle H_A \rangle < H_{max} < 1{,}0 \langle H_A \rangle$, hai que diminuír σ_K. Isto é debido a que o campo aplicado non é capaz de abrir os ciclos das partículas que teñen maior anisotropía. Por último, se o campo aplicado é tal que $H_{max} > 1{,}0 \langle H_A \rangle$, todas as NPMs da mostra son capaces de liberar enerxía e o efecto de variar σ_K é só apreciable a nivel local. Despois utilízase de novo a desviación estándar σ_{HL} para calcular canto se desvía a calor local da global para diferentes amplitudes do campo aplicado. Móstrase tamén a desviación estándar normalizada coa enerxía disipada global. Isto permite ter en conta que a dispersión en calor local está vinculada a un valor promedio e que a relevancia de σ_{HL} depende del. Esta información utilízase para mostrar como ter unha HMN máis segura (é dicir, cunha dispersión en calor local menor) variando a amplitude de campo ou modificando a constante de anisotropía.

Unha vez tendo discutido de forma xeral os resultados máis destacables desta tese, finalízase resaltando as conclusións principais deste traballo. A primeira é que incluso un grao baixo de polidispersidade, xa sexa en tamaño ou en anisotropía, pode afectar de maneira importante á disipación local. A aparición dunha ampla variedade de focos de calor local constitúe un reto para deseñar un tratamento de HMN eficaz e seguro xa que algunhas partes do tumor a tratar quentaríanse en exceso, podendo ferir o tecido san circundante, e outras non o farían o suficiente, deixando células cancerosas sen danar. Demóstrase tamén que é necesario diferenciar entre calor global e eficacia da HMN: alcanzar valores altos de SAR global non implica necesariamente un tratamento máis efectivo debido á dispersión de calor local. A dispersión local, que se cuantificou coa desviación estándar, pode chegar a ser moi elevada, alcanzando ou incluso superando o 100 % do valor global promedio. A temperatura e o tamaño promedio son parámetros relevantes a ter en conta cando hai polidispersidade en tamaño e a amplitude do campo aplicado é chave cando hai polidispersidade en anisotropía. Ilústrase como os parámetros normalizados poden ser útiles para atopar un tamaño promedio de partícula adecuado que limite a dispersión de calor local tendo en conta o grao de polidispersidade da mostra. Para non superar o límite desexado, o máis sinxelo é diminuír o tamaño das NPMs, pero isto reduce tamén a enerxía liberada. Polo tanto, debe atoparse un equilibrio entre ambos efectos para ter un tratamento de HMN tanto efectivo como seguro. Mostrouse tamén un procedemento teórico no que a información sobre a calor local se usa para atopar o tamaño promedio do sistema que permite ter o maior

número de NPMs disipando nun intervalo de SAR de interese en función da polidispersidade en tamaño. No que respecta aos efectos da anisotropía, a súa dispersión e á amplitude do campo aplicado, diferenciáronse tres réximes de campo nos que se observan distintos efectos na calor disipada segundo a relación entre estes parámetros. Para rematar e seguindo o último resultado mencionado, conclúese que para ter unha distribución de calor local o máis homoxénea posible, é preferible traballar en condicións de ciclos de histérese maiores. Isto pódese conseguir aumentando a amplitude do campo aplicado, aínda que se houbera limitacións neste aspecto, sería recomendable escoller NPMs cunha constante de anisotropía baixa.

REFERENCES

[1] Daniel Ortega and Quentin A Pankhurst. Magnetic hyperthermia. *Nanoscience*, 1(60):60–88, 2013.

[2] Silvio Dutz and Rudolf Hergt. Magnetic nanoparticle heating and heat transfer on a microscale: basic principles, realities and physical limitations of hyperthermia for tumour therapy. *International Journal of Hyperthermia*, 29(8):790–800, 2013.

[3] Chanchala D Kaddi, John H Phan, and May D Wang. Computational nanomedicine: modeling of nanoparticle-mediated hyperthermal cancer therapy. *Nanomedicine*, 8(8):1323–1333, 2013.

[4] Elio Alberto Perigo, Gauvin Hemery, Olivier Sandre, Daniel Ortega, Eneko Garaio, Fernando Plazaola, and Francisco Jose Teran. Fundamentals and advances in magnetic hyperthermia. *Applied Physics Reviews*, 2(4):041302, 2015.

[5] Miriam Colombo, Susana Carregal-Romero, Maria F Casula, Lucia Gutierrez, Maria P Morales, Ingrid B Boehm, Johannes T Heverhagen, Davide Prosperi, and Wolfgang J Parak. Biological applications of magnetic nanoparticles. *Chemical Society Reviews*, 41(11):4306–4334, 2012.

[6] Silvio Dutz and Rudolf Hergt. Magnetic particle hyperthermia—a promising tumour therapy? *Nanotechnology*, 25(45):452001, 2014.

[7] Kannan M Krishnan. Biomedical nanomagnetics: a spin through possibilities in imaging, diagnostics, and therapy. *IEEE transactions on magnetics*, 46(7):2523–2558, 2010.

[8] Morteza Mahmoudi, Shilpa Sant, Ben Wang, Sophie Laurent, and Tapas Sen. Superparamagnetic iron oxide nanoparticles (spions): development, surface modification and applications in chemotherapy. *Advanced drug delivery reviews*, 63(1-2):24–46, 2011.

[9] Stephen E Barry. Challenges in the development of magnetic particles for therapeutic applications. *International Journal of Hyperthermia*, 24(6):451–466, 2008.

[10] Pedro Tartaj, Maria del Puerto Morales, Sabino Veintemillas-Verdaguer, Teresita González-Carreño, and Carlos J Serna. The preparation of magnetic nanoparticles for applications in biomedicine. *Journal of physics D: Applied physics*, 36(13):R182, 2003.

[11] Daishun Ling and Taeghwan Hyeon. Chemical design of biocompatible iron oxide nanoparticles for medical applications. *Small*, 9(9-10):1450–1466, 2013.

[12] G Vallejo-Fernandez and K O'Grady. Effect of the distribution of anisotropy constants on hysteresis losses for magnetic hyperthermia applications. *Applied Physics Letters*, 103(14):142417, 2013.

[13] Yan Geng, Paul Dalhaimer, Shenshen Cai, Richard Tsai, Manorama Tewari, Tamara Minko, and Dennis E Discher. Shape effects of filaments versus spherical particles in flow and drug delivery. *Nature nanotechnology*, 2(4):249, 2007.

[14] Carlos Martinez-Boubeta, Konstantinos Simeonidis, Antonios Makridis, Makis Angelakeris, Oscar Iglesias, Pablo Guardia, Andreu Cabot, Lluis Yedra, Sonia Estradé, Francesca Peiró, et al. Learning from nature to improve the heat generation of iron-oxide nanoparticles for magnetic hyperthermia applications. *Scientific reports*, 3:1652, 2013.

[15] Raja Das, Javier Alonso, Zohreh Nemati Porshokouh, Vijaysankar Kalappattil, David Torres, Manh-Huong Phan, Eneko Garaio, Jose Angel Garcia, Jose Luis Sanchez Llamazares, and Hariharan Srikanth. Tunable high aspect ratio iron oxide nanorods for enhanced hyperthermia. *The Journal of Physical Chemistry C*, 120(18):10086–10093, 2016.

[16] Carlos Martinez-Boubeta, Konstantinos Simeonidis, David Serantes, Iván Conde-Leborán, Ioannis Kazakis, George Stefanou, Luis Peña, Regina Galceran, Lluis Balcells, Claude Monty, et al. Adjustable hyperthermia response of self-assembled ferromagnetic fe-mgo core–shell nanoparticles by tuning dipole–dipole interactions. *Advanced Functional Materials*, 22(17):3737–3744, 2012.

[17] Julian Carrey, Boubker Mehdaoui, and Marc Respaud. Simple models for dynamic hysteresis loop calculations of magnetic single-domain nanoparticles: Application to magnetic hyperthermia optimization. *Journal of Applied Physics*, 109(8):083921, 2011.

[18] Ihab M Obaidat, Bashar Issa, and Yousef Haik. Magnetic properties of magnetic nanoparticles for efficient hyperthermia. *Nanomaterials*, 5(1):63–89, 2015.

[19] Silvio Dutz, Robert Müller, Dietmar Eberbeck, Ingrid Hilger, and Matthias Zeisberger. Magnetic nanoparticles adapted for specific biomedical applications. *Biomedical Engineering/Biomedizinische Technik*, 60(5):405–416, 2015.

[20] Edmund Clifton Stoner and EP Wohlfarth. A mechanism of magnetic hysteresis in heterogeneous alloys. *Phil. Trans. R. Soc. Lond. A*, 240(826):599–642, 1948.

[21] Ivan Conde-Leboran, Daniel Baldomir, Carlos Martinez-Boubeta, Oksana Chubykalo-Fesenko, María del Puerto Morales, Gorka Salas, David Cabrera, Julio Camarero, Francisco J Teran, and David Serantes. A single picture explains diversity of hyperthermia response of magnetic nanoparticles. *The Journal of Physical Chemistry C*, 119(27):15698–15706, 2015.

[22] Ainhoa Urtizberea, Eva Natividad, Ana Arizaga, Miguel Castro, and Arturo Mediano. Specific absorption rates and magnetic properties of ferrofluids with interaction effects at low concentrations. *The Journal of Physical Chemistry C*, 114(11):4916–4922, 2010.

[23] Christian Haase and Ulrich Nowak. Role of dipole-dipole interactions for hyperthermia heating of magnetic nanoparticle ensembles. *Physical Review B*, 85(4):045435, 2012.

[24] Pham Hoai Linh, Pham Van Thach, Nguyen Anh Tuan, Nguyen Chi Thuan, Do Hung Manh, Nguyen Xuan Phuc, and Le Van Hong. Magnetic fluid based on fe 3 o 4 nanoparticles: Preparation and hyperthermia application. *Journal of Physics: Conference Series*, 187(1):012069, 2009.

[25] Minhong Jeun, Seongtae Bae, Asahi Tomitaka, Yasushi Takemura, Ki Ho Park, Sun Ha Paek, and Kyung-Won Chung. Effects of particle dipole interaction on the ac magnetically induced heating characteristics of ferrite nanoparticles for hyperthermia. *Applied physics letters*, 95(8):082501, 2009.

[26] CL Dennis, AJ Jackson, JA Borchers, R Ivkov, AR Foreman, JW Lau, E Goernitz, and C Gruettner. The influence of collective behavior on the magnetic and heating properties of iron oxide nanoparticles. *Journal of Applied Physics*, 103(7):07A319, 2008.

[27] B Mehdaoui, RP Tan, A Meffre, J Carrey, S Lachaize, B Chaudret, and M Respaud. Increase of magnetic hyperthermia efficiency due to dipolar interactions in low-anisotropy magnetic nanoparticles: Theoretical and experimental results. *Physical Review B*, 87(17):174419, 2013.

[28] David Serantes, Konstantinos Simeonidis, Makis Angelakeris, Oksana Chubykalo-Fesenko, Marzia Marciello, Maria Del Puerto Morales, Daniel Baldomir, and Carlos Martinez-Boubeta. Multiplying magnetic hyperthermia response by nanoparticle assembling. *The Journal of Physical Chemistry C*, 118(11):5927–5934, 2014.

[29] Nguyen Lan Tran and Hoang Hai Tran. Role of the poly-dispersity and the dipolar interaction in magnetic nanoparticle systems: Monte carlo study. *Journal of Non-Crystalline Solids*, 357(3):996–999, 2011.

[30] Gabriel T Landi. Role of dipolar interaction in magnetic hyperthermia. *Physical Review B*, 89(1):014403, 2014.

[31] Riccardo Di Corato, Ana Espinosa, Lenaic Lartigue, Mickael Tharaud, Sophie Chat, Teresa Pellegrino, Christine Ménager, Florence Gazeau, and Claire Wilhelm. Magnetic hyperthermia efficiency in the cellular environment for different nanoparticle designs. *Biomaterials*, 35(24):6400–6411, 2014.

[32] Louis Néel. Théorie du traînage magnétique des ferromagnétiques en grains fins avec applications aux terres cuites. *Ann. géophys.*, 5:99–136, 1949.

[33] William Fuller Brown Jr. Thermal fluctuations of a single-domain particle. *Physical Review*, 130(5):1677, 1963.

[34] MI Shliomis. Magnetic fluids. *Physics-Uspekhi*, 17(2):153–169, 1974.

[35] SH Chung, A Hoffmann, SD Bader, C Liu, B Kay, L Makowski, and L Chen. Biological sensors based on brownian relaxation of magnetic nanoparticles. *Applied physics letters*, 85(14):2971–2973, 2004.

[36] Iván Conde-Leborán, David Serantes, and Daniel Baldomir. Orientation of the magnetization easy axes of interacting nanoparticles: Influence on the hyperthermia properties. *Journal of Magnetism and Magnetic Materials*, 380:321–324, 2015.

[37] Konstantinos Simeonidis, M Puerto Morales, Marzia Marciello, Makis Angelakeris, Patricia de La Presa, Ana Lazaro-Carrillo, Andrea Tabero, Angeles Villanueva, Oksana Chubykalo-Fesenko, and David Serantes. In-situ particles reorientation during magnetic hyperthermia application: Shape matters twice. *Scientific reports*, 6:38382, 2016.

[38] William J Atkinson, Ivan A Brezovich, and Dev P Chakraborty. Usable frequencies in hyperthermia with thermal seeds. *IEEE Transactions on Biomedical Engineering*, 31(1):70–75, 1984.

[39] Burghard Thiesen and Andreas Jordan. Clinical applications of magnetic nanoparticles for hyperthermia. *International journal of hyperthermia*, 24(6):467–474, 2008.

[40] Susanne Kossatz, Robert Ludwig, Heidi Dähring, Volker Ettelt, Gabriella Rimkus, Marzia Marciello, Gorka Salas, Vijay Patel, Francisco J Teran, and Ingrid Hilger. High therapeutic efficiency of magnetic hyperthermia in xenograft models achieved with moderate temperature dosages in the tumor area. *Pharmaceutical research*, 31(12):3274–3288, 2014.

[41] MagForce AG. https://www.magforce.com/en/home.html. [Online; accessed 28-August-2018].

[42] Klaus Maier-Hauff, Ronny Rothe, Regina Scholz, Uwe Gneveckow, Peter Wust, Burghard Thiesen, Annelie Feussner, Andreas von Deimling, Norbert Waldoefner, Roland Felix, et al. Intracranial thermotherapy using magnetic nanoparticles combined with external beam radiotherapy: results of a feasibility study on patients with glioblastoma multiforme. *Journal of neuro-oncology*, 81(1):53–60, 2007.

[43] Klaus Maier-Hauff, Frank Ulrich, Dirk Nestler, Hendrik Niehoff, Peter Wust, Burghard Thiesen, Helmut Orawa, Volker Budach, and Andreas Jordan. Efficacy and safety of intratumoral thermotherapy using magnetic iron-oxide nanoparticles combined with external beam radiotherapy on patients with recurrent glioblastoma multiforme. *Journal of neuro-oncology*, 103(2):317–324, 2011.

[44] Frank KH van Landeghem, K Maier-Hauff, A Jordan, Karl-Titus Hoffmann, U Gneveckow, R Scholz, B Thiesen, W Brück, and A Von Deimling. Post-mortem studies in glioblastoma patients treated with thermotherapy using magnetic nanoparticles. *Biomaterials*, 30(1):52–57, 2009.

[45] Manfred Johannsen, U Gneveckow, L Eckelt, A Feussner, N Waldöfner, R Scholz, S Deger, P Wust, SA Loening, and A Jordan. Clinical hyperthermia of prostate cancer using magnetic nanoparticles: presentation of a new interstitial technique. *International journal of hyperthermia*, 21(7):637–647, 2005.

[46] Manfred Johannsen, Uwe Gneveckow, Burghard Thiesen, Kasra Taymoorian, Chie Hee Cho, Norbert Waldöfner, Regina Scholz, Andreas Jordan, Stefan A Loening, and Peter Wust. Thermotherapy of prostate cancer using magnetic nanoparticles: feasibility, imaging, and three-dimensional temperature distribution. *European urology*, 52(6):1653–1662, 2007.

[47] M Johannsen, U Gneveckow, K Taymoorian, B Thiesen, N Waldöfner, R Scholz, K Jung, A Jordan, P Wust, and SA Loening. Morbidity and quality of life during thermotherapy using magnetic nanoparticles in locally recurrent prostate cancer: results of a prospective phase i trial. *International Journal of Hyperthermia*, 23(3):315–323, 2007.

[48] Peter Wust, Uwe Gneveckow, > Peter Wust, Uwe Gneveckow, Manfred Johannsen, Dirk Böhmer, Thomas Henkel, Frank Kahmann, Jalid Sehouli, Roland Felix, et al. Magnetic nanoparticles for interstitial thermotherapy–feasibility, tolerance and achieved temperatures. *International Journal of Hyperthermia*, 22(8):673–685, 2006.

[49] Magnetic Nanoparticle Thermoablation-Retention and Maintenance in the Prostate: A Phase 0 Study in Men. https://www.clinicaltrials.gov/ct2/show/NCT02033447. [Online; accessed 05-September-2018].

[50] Phase I study for immuno-hyperthermia against recurrent subcutaneous tumor using cationic magnetoliposome and alternative magnetic field irradiation. https://upload.umin.ac.jp/cgi-open-bin/ctr_e/ctr_view.cgi?recptno=R000003291. [Online; accessed 06-September-2018].

[51] DOI: 10.1039/c5cp04539h. http://pubs.rsc.org/en/Content/ArticleLanding/2015/CP/C5CP04539H#!divAbstract.

[52] Mar Creixell, Ana C Bohorquez, Madeline Torres-Lugo, and Carlos Rinaldi. Egfr-targeted magnetic nanoparticle heaters kill cancer cells without a perceptible temperature rise. *ACS nano*, 5(9):7124–7129, 2011.

[53] L Asin, MR Ibarra, A Tres, and GF Goya. Controlled cell death by magnetic hyperthermia: effects of exposure time, field amplitude, and nanoparticle concentration. *Pharmaceutical research*, 29(5):1319–1327, 2012.

[54] Valeria Grazú, Ariel Mariano Silber, M Moros, L Asin, TE Torres, C Marquina, MR Ibarra, and GF Goya. Application of magnetically induced hyperthermia in the model protozoan crithidia fasciculata as a potential therapy against parasitic infections. *International journal of nanomedicine*, 7:5351, 2012.

[55] A Villanueva, P De La Presa, JM Alonso, T Rueda, A Martinez, P Crespo, MP Morales, MA Gonzalez-Fernandez, J Valdes, and G Rivero. Hyperthermia hela cell treatment with silica-coated manganese oxide nanoparticles. *The Journal of Physical Chemistry C*, 114(5):1976–1981, 2010.

[56] Jorge T Dias, María Moros, Pablo del Pino, Sara Rivera, Valeria Grazú, and Jesus M de la Fuente. Dna as a molecular local thermal probe for the analysis of magnetic hyperthermia. *Angewandte Chemie International Edition*, 52(44):11526–11529, 2013.

[57] Andreas Riedinger, Pablo Guardia, Alberto Curcio, Miguel A Garcia, Roberto Cingolani, Liberato Manna, and Teresa Pellegrino. Subnanometer local temperature probing and remotely controlled drug release based on azo-functionalized iron oxide nanoparticles. *Nano letters*, 13(6):2399–2406, 2013.

[58] Georg Kucsko, PC Maurer, Norman Ying Yao, MICHAEL Kubo, HJ Noh, PK Lo, Hongkun Park, and Mikhail D Lukin. Nanometre-scale thermometry in a living cell. *Nature*, 500(7460):54, 2013.

[59] Nicholas Metropolis, Arianna W Rosenbluth, Marshall N Rosenbluth, Augusta H Teller, and Edward Teller. Equation of state calculations by fast computing machines. *The journal of chemical physics*, 21(6):1087–1092, 1953.

[60] D Serantes, D Baldomir, C Martinez-Boubeta, K Simeonidis, M Angelakeris, E Natividad, M Castro, A Mediano, D-X Chen, A Sanchez, et al. Influence of dipolar interactions on hyperthermia properties of ferromagnetic particles. *Journal of Applied Physics*, 108(7):073918, 2010.

[61] Sophie Laurent, Silvio Dutz, Urs O Häfeli, and Morteza Mahmoudi. Magnetic fluid hyperthermia: focus on superparamagnetic iron oxide nanoparticles. *Advances in colloid and interface science*, 166(1-2):8–23, 2011.

[62] Marcela Gonzales-Weimuller, Matthias Zeisberger, and Kannan M Krishnan. Size-dependant heating rates of iron oxide nanoparticles for magnetic fluid hyperthermia. *Journal of magnetism and magnetic materials*, 321(13):1947–1950, 2009.

[63] Eneko Garaio, Olivier Sandre, Juan-Mari Collantes, Jose Angel Garcia, Stéphane Mornet, and Fernando Plazaola. Specific absorption rate dependence on temperature in magnetic field hyperthermia measured by dynamic hysteresis losses (ac magnetometry). *Nanotechnology*, 26(1):015704, 2014.

[64] Silvio Dutz, Melanie Kettering, Ingrid Hilger, Robert Müller, and Matthias Zeisberger. Magnetic multicore nanoparticles for hyperthermia—influence of particle immobilization in tumour tissue on magnetic properties. *Nanotechnology*, 22(26):265102, 2011.

[65] Dalibor Soukup, Sandhya Moise, Eva Céspedes, Jon Dobson, and Neil D Telling. In situ measurement of magnetization relaxation of internalized nanoparticles in live cells. *Acs Nano*, 9(1):231–240, 2015.

[66] R Müller, S Dutz, A Neeb, ACB Cato, and M Zeisberger. Magnetic heating effect of nanoparticles with different sizes and size distributions. *Journal of Magnetism and Magnetic Materials*, 328:80–85, 2013.

[67] G Hassnain Jaffari, Thomas Ekiert, KM Unruh, and S Ismat Shah. Effect of particle size distribution on the magnetic properties γ-fe2o3 nanoparticles. *Materials Science and Engineering: B*, 177(12):935–941, 2012.

[68] P De la Presa, Y Luengo, M Multigner, R Costo, MP Morales, G Rivero, and A Hernando. Study of heating efficiency as a function of concentration, size, and applied field in γ-fe2o3 nanoparticles. *The Journal of Physical Chemistry C*, 116(48):25602–25610, 2012.

[69] Boubker Mehdaoui, Anca Meffre, Julian Carrey, Sébastien Lachaize, Lise-Marie Lacroix, Michel Gougeon, Bruno Chaudret, and Marc Respaud. Optimal size of nanoparticles for magnetic hyperthermia: a combined theoretical and experimental study. *Advanced Functional Materials*, 21(23):4573–4581, 2011.

[70] RD Zysler, D Fiorani, and AM Testa. Investigation of magnetic properties of interacting fe2o3 nanoparticles. *Journal of magnetism and magnetic materials*, 224(1):5–11, 2001.

[71] Ulrich Nowak, Roy W Chantrell, and EC Kennedy. Monte carlo simulation with time step quantification in terms of langevin dynamics. *Physical review letters*, 84(1):163, 2000.

[72] Oksana Chubykalo, Ulrich Nowak, Roman Smirnov-Rueda, MA Wongsam, Roy W Chantrell, and JM Gonzalez. Monte carlo technique with a quantified time step: Application to the motion of magnetic moments. *Physical Review B*, 67(6):064422, 2003.

[73] W Keith Hastings. Monte carlo sampling methods using markov chains and their applications. *Biometrika*, 57(1), 1970.

[74] David P Landau and Kurt Binder. *A guide to Monte Carlo simulations in statistical physics*. Cambridge university press, 2014.

[75] Ronald E Rosensweig. Heating magnetic fluid with alternating magnetic field. *Journal of magnetism and magnetic materials*, 252:370–374, 2002.

[76] LL Castro, MF Da Silva, AF Bakuzis, and R Miotto. Aggregate formation on polydisperse ferrofluids: a monte carlo analysis. *Journal of magnetism and magnetic materials*, 293(1):553–558, 2005.

[77] Vincent Russier, Caroline De Montferrand, Yoann Lalatonne, and Laurence Motte. Size and polydispersity effect on the magnetization of densely packed magnetic nanoparticles. *Journal of Applied Physics*, 112(7):073926, 2012.

[78] Amit P Khandhar, R Matthew Ferguson, and Kannan M Krishnan. Monodispersed magnetite nanoparticles optimized for magnetic fluid hyperthermia: Implications in biological systems. *Journal of applied physics*, 109(7):07B310, 2011.

[79] Gorka Salas, Cintia Casado, Francisco J Teran, Rodolfo Miranda, Carlos J Serna, and M Puerto Morales. Controlled synthesis of uniform magnetite nanocrystals with high-quality properties for biomedical applications. *Journal of Materials Chemistry*, 22(39):21065–21075, 2012.

[80] DOI: 10.1039/c6sm01910b. http://pubs.rsc.org/en/content/articlelanding/2016/sm/c6sm01910b/unauth#!divAbstract.

[81] Rudolf Hergt, Silvio Dutz, Robert Müller, and Matthias Zeisberger. Magnetic particle hyperthermia: nanoparticle magnetism and materials development for cancer therapy. *Journal of Physics: Condensed Matter*, 18(38):S2919, 2006.

[82] MM Cruz, LP Ferreira, J Ramos, SG Mendo, AF Alves, M Godinho, and MD Carvalho. Enhanced magnetic hyperthermia of cofe2o4 and mnfe2o4 nanoparticles. *Journal of Alloys and Compounds*, 703:370–380, 2017.

[83] G Vallejo-Fernandez, O Whear, AG Roca, S Hussain, J Timmis, V Patel, and K O'Grady. Mechanisms of hyperthermia in magnetic nanoparticles. *Journal of Physics D: Applied Physics*, 46(31):312001, 2013.

[84] S Ruta, R Chantrell, and O Hovorka. Unified model of hyperthermia via hysteresis heating in systems of interacting magnetic nanoparticles. *Scientific reports*, 5:9090, 2015.

[85] Shuo Gu, Weidong He, Ming Zhang, Taisen Zhuang, Yi Jin, Hatem ElBidweihy, Yiwu Mao, James H Dickerson, Michael J Wagner, Edward Della Torre, et al. Physical justification for negative remanent magnetization in homogeneous nanoparticles. *Scientific reports*, 4:6267, 2014.

[86] Beatriz Mora, Nastassia Soriano, Carolina Redondo, Alberto Arteche, David Navas, and Rafael Morales. Engineering magnetic nanostructures with inverse hysteresis loops. *Nano Research*, 9(8):2347–2353, 2016.

[87] Petru Andrei and Mihai Dimian. Clockwise jiles–atherton hysteresis model. *IEEE Transactions on Magnetics*, 49(7):3183–3186, 2013.

[88] Juan Ruben Gomez-Solano, Christoph July, Jakob Mehl, and Clemens Bechinger. Non-equilibrium work distribution for interacting colloidal particles under friction. *New Journal of Physics*, 17(4):045026, 2015.

[89] Pablo Nieves, David Serantes, Unai Atxitia, and Oksana Chubykalo-Fesenko. Quantum landau-lifshitz-bloch equation and its comparison with the classical case. *Physical Review B*, 90(10):104428, 2014.

[90] P Nieves, D Serantes, and O Chubykalo-Fesenko. Self-consistent description of spin-phonon dynamics in ferromagnets. *Physical Review B*, 94(1):014409, 2016.